Differential predictive value of resident memory CD8⁺T cell subpopulations in non-small-cell lung cancer patients treated by immunotherapy

Predictive value of resident memory CD8⁺T cells

Léa Paolini[1‡], Thi Tran[1‡], Stéphanie Corgnac[3*], Jean-Philippe Villemin[4*], Marie Wislez[5*], Jennifer Arrondeau[6], Ludger Johannes[7], Jonathan Ulmer[7], Louis-Victorien Vieillard[1*], Joséphine Pineau[1,2], Alain Gey[1,2] , Valentin Quiniou[8], Pierre Barennes [8], Hang Phuong Pham[8], Nadège Gruel[9,10], Milena Hasan[11], Valentina Libri[11], Sébastien Mella [11], Sixtine De Percin[6], Pascaline Boudou-Rouquette[6], Isabelle Cremer[12], Hélène Blons[13], Karen Leroy[12,13], Pierre Laurent-Puig[13], Hortense De Saint Basile[1,14], Laure Gibault [15], Patrice Ravel [4] , Fathia Mami-Chouaib[3], François Goldwasser[6] , Elizabeth Fabre[1,14], Diane Damotte[12,16], Eric Tartour[1,2#]

[1] Université ParisCité, INSERM, PARCC, Paris, France

[2] APHP, Hôpital Européen Georges Pompidou (HEGP) and Hôpital Necker, Paris. Department of Immunology

[3] INSERM UMR 1186, Gustave Roussy, Fac. de Médecine - Univ. Paris-Sud, Université Paris-Saclay, Villejuif, France

[4] Institut de Recherche en Cancérologie de Montpellier-INSERM U1194, Montpellier, France.

[5] Université de Paris Cité, faculté de médecine, Centre de recherche des Cordeliers, Inserm, AP-HP Centre, hôpital Cochin, service de pneumologie, unité d'oncologie thoracique, Paris.

[6] Department of Medical Oncology, Cochin Hospital, Paris Cancer Institute CARPEM, Université Paris Cité, APHP, Paris.

[7] Cellular and Chemical Biology Unit, Institut Curie, 75248 Paris Cedex 05, France

[8] Parean biotechnologies, St-Malo, France..

[9]INSERM U830, Equipe Labellis_ee Ligue Nationale Contre le Cancer, Diversity and Plasticity of Childhood Tumours Lab, PSL Research University, Institut Curie Research Center, Paris, France.

[10] Department of Translational Research, PSL Research University, Institut Curie Research Center, Paris, France

[11] Cytometry and Biomarkers UTechS, Center for Translational Science, Institut Pasteur, Paris, France.

[12] Centre de Recherche des Cordeliers, INSERM, Sorbonne Université, Université de Paris Cité, Paris.

[13] Department of Biochemistry, Unit of Pharmacogenetics and Molecular Oncology, HEGP, Paris

[14] APHP, Department of Thoracic Oncology, HEGP, Paris.

[15]APHP Department of Pathology HEGP. Paris, France.

[16] APHP Department of Pathology, Cochin Hospital, Groupe Hospitalier Paris Centre, Paris Cancer Institute CARPEM, Université Paris Cité.

‡ Co-first author

* contributed equally (LP and TT participate in the conception of the work, they conduct experiments and acquired, analyzed and interpret the data as well as participation in the first drafting of the work. LP is first as she provided the figure 4 and 5 which could be considered slightly more important for the conclusion of the study)

Corresponding author : Eric Tartour. Hôpital Européen Georges Pompidou. 20 Rue Leblanc 75015 Paris. eric.tartour@aphp.fr

Keywords : Resident memory T cells, NSCLC, Immunotherapy, Biomarker

Abstract (175 words)

A high density of resident memory T cells (T_{RM}) in tumors correlates with improved clinical outcomes in immunotherapy-treated patients. However, in preclinical models, only some subpopulations of T_{RM} are associated with cancer vaccine efficacy.

We identified two main T_{RM} subpopulations in tumor-infiltrating lymphocytes derived from non-small cell lung cancer (NSCLC) patients: one co-expressing CD103 and CD49a (DP), and the other expressing only CD49a (MP); both exhibiting additional T_{RM} surface markers like CD69. DP T_{RM} exhibited greater functionality compared to MP T_{RM}. Analysis of T-cell receptor (TCR) repertoire and of the stemness marker TCF-1 revealed shared TCRs between populations, with the MP subset appearing more progenitor-like phenotype. In two NSCLC patient cohorts, only DP T_{RM} predicted PD-1 blockade response. Multivariate analysis, including various biomarkers (CD8, $TCF1^+CD8^+$T cells, and PD-L1) associated with responses to anti-PD(L)1, showed that only intra-tumoral infiltration by DP T_{RM} remained significant. This study highlights the non-equivalence of T_{RM} populations and emphasizes the importance of distinguishing between them to better define their role in antitumor immunity and as a biomarker of response to immunotherapy.

Introduction

More than two decades ago, pioneering work on vesicular stomatitis virus and *Listeria monocytogenes* revealed the presence and persistence of noncirculating resident memory T cells (T_{RM}) in nonlymphoid organs after the resolution of the primary infection (Masopust, Vezys et al., 2001). It rapidly became apparent that these T_{RM} constituted a specific lineage associated with a profile of transcription factors including Blimp1, Runx3, and Notch family proteins (Hombrink, Helbig et al., 2016). In terms of their phenotype, these T_{RM} express core markers such as CD69, CD103, and CD49a, together with the loss of expression of other markers such as CD62L, CCR7, S1PR1, and KLF2, favoring the persistence of these cells within tissues (Kumar, Ma et al., 2017, Mami-Chouaib, Blanc et al., 2018). T_{RM} have innate-like "sensing and alarming" properties that enable them to recruit other immune cells to control microbial infections (Ariotti, Hogenbirk et al., 2014, Ge, Monk et al., 2019, Schenkel & Masopust, 2014). As they are located at the site of inflammation in the tissues, T_{RM} respond much more rapidly to reinfection and provide superior protection compared to circulating memory cells, including central memory and effector memory T cells (Ariotti et al., 2014, Iijima & Iwasaki, 2014, Schenkel & Masopust, 2014).

In a range of preclinical cancer models, we have shown that T_{RM} are required for the efficacy of anti-tumor vaccines against mucosal tumors such as lung and head and neck cancer (Nizard, Roussel et al., 2017, Sandoval, Terme et al., 2013). T_{RM} can also activate dendritic cells (DCs) to increase the numbers of tumor-specific $CD8^+$ T cells, conferring protection against tumor rechallenge (Menares, Galvez-Cancino et al., 2019). In humans, high levels of intratumoral T_{RM} infiltration have been associated with better clinical outcomes in multiple solid tumors including lung, melanoma, bladder, breast, cervical, ovarian, endometrial, gastric, and colorectal cancers receiving standard-of-care treatments (Djenidi, Adam et al., 2015, Ganesan, Clarke et al., 2017, Nizard et al., 2017, Okla, Farber et al., 2021, Wang, Wu et al., 2015). More recently in humans, correlative studies in non-small cell lung cancer (NSCLC), bladder cancer, and melanoma have revealed an association between tumor infiltration by $CD8^+$ T cells with a resident phenotype before immunotherapy and responses to immune checkpoint blockade (Attrill, Owen et al., 2022, Banchereau, Chitre et al., 2021, Corgnac, Malenica et al., 2020, Zitti, Hoffer et al., 2023).

To explain this predictive role of T_{RM} during immunotherapy, various groups have shown that during neoadjuvant treatment in breast and head and neck cancer, $CD8^+$ tumor-infiltrating lymphocytes (TILs) with a tissue-resident phenotype expand and are characterized by a gene expression program related to activation, cytotoxicity, and effector functionality (Bassez, Vos et al., 2021, Luoma, Suo et al., 2022). The same expansion of $CD8^+$ T_{RM} has been observed after anti-PD-1/PD-L1 monotherapy or combined anti-CTLA-4 treatment in melanoma, lung, breast, and esophageal cancer (Corgnac et al., 2020, Edwards, Wilmott et al., 2018, Jaiswal,

Verma et al., 2022, Virassamy, Caramia et al., 2023). The role of T_{RM} as immunotherapeutic targets raises the possibility that other effectors recruited secondarily or present in the blood may play a role in the efficacy of immunotherapy (Yost, Satpathy et al., 2019).

Given the anti-tumor role of T_{RM} and their prognostic and predictive value in the context of patient responses to immunotherapy, the issue of optimal strategies for inducing or increasing this population is becoming a major challenge in immuno-oncology. In preclinical models, we have shown that the nasal route, but not the muscular route, induces T_{RM} with a $CD103^+CD49a^+CD69^+$ phenotype (Nizard et al., 2017, Sandoval et al., 2013). This induction was associated with the inhibition of the growth of lung or head and neck tumors. In infectious and oncological models, other groups have also documented a correlation between the preferential ability of mucosal immunization to induce T_{RM} expansion and protection against the development of cancers and viral infections (Jeyanathan, Fritz et al., 2022, Stewart, Counoupas et al., 2022, Sun, Peng et al., 2016). However, other studies based on vaccinations using systemically administered recombinant viral vectors have shown that T_{RM} can be induced in the lungs (Douguet, Fert et al., 2023). This result may be explained by the use of viruses that enable vaccine dissemination in the pulmonary or head and neck compartments. However, mRNA-based vaccinations have also been shown to induce T_{RM} when administered via the intramuscular (i.m.) route, but the cells induced in this context generally express CD69 or CD49a without any concomitant CD103 expression (Kunzli, O'Flanagan et al., 2022). The fact that different sub-populations of T_{RM} exist with differing core marker (CD103, CD49a, CD69) expression patterns has been reported in various tissues, and this effect has sometimes been linked to the different functions of these cells (Cheuk, Schlums et al., 2017). Although CD103 is considered a hallmark of T_{RM}, persistent CD103-negative T_{RM} have also been described in tissues. In contrast with CD103+ T_{RM}, these cells were able to develop in a TGFβ-independent manner (Bergsbaken & Bevan, 2015, Schenkel, Fraser et al., 2014, Steinert, Schenkel et al., 2015).

In this work, we aimed to better characterize these different T_{RM} subpopulations in mice and humans and to determine whether they play distinct roles as predictors of responses to immunotherapy in patients with NSCLC.

RESULTS

1. Different immunization routes give rise to distinct subpopulations of resident memory CD8$^+$T lymphocytes.

Our previous work had shown that only the intranasal (i.n) immunization route induced resident memory CD103-expressing CD8$^+$T cells in bronchoalveolar lavage fluid (BAL), and this mucosal immunization route was associated with tumor rejection (Nizard et al., 2017). In recent years, it has emerged that there are different T_{RM} subpopulations defined by the markers CD103, CD49a, and CD69 (Mami-Chouaib et al., 2018). Only i.n. vaccination with the STxB-E7 vaccine combined with αGalCer induced D^b-restricted $E7_{49-57}$ peptide-specific CD8$^+$T cells co-expressing CD103 and CD49a in the BAL (Fig. 1A). In contrast, the i.m. route also induced E7-specific CD8$^+$ T cells expressing CD49a but not CD103 (Fig. 1A). Both CD103$^+$CD49a$^+$ and CD103^{neg}CD49a$^+$CD8$^+$ T cell populations induced by the i.n route expressed high levels of CD69 (For CD103$^+$CD49a$^+$: Mean 94.82% $\pm$ 1.86% and for CD103^{neg}CD49a$^+$ Mean: 95.5% $\pm$ 1.49%) (Fig. 1A, lower right), whereas the frequency of CD8$^+$ T cells specific for E7 and expressing neither CD103 nor CD49a, which are considered to be effector T cells, exhibited weaker CD69 expression (Mean 49.24% $\pm$ 10.24%)(Fig. 1A, lower right). Immunization via the i.n. route induced a marginal CD103$^+$CD49a$^-$T cell population (< 5%)(Fig. 1)

It should be noted that i.m.-induced CD49a$^+$CD103$^-$CD8$^+$T cells were less likely to express CD69 as compared to i.n.-induced ones (Mean: 68.4% $\pm$ 11.6%)(Fig. 1A, upper right), but their numbers were equivalent in the BAL irrespective of the immunization route (Fig. 1B). These results were replicated by analyzing the same resident memory CD8$^+$ T cell subpopulations in lung parenchyma after i.m or i.n vaccination (Fig. S2 A,B).

Similarly, using another vaccine system consisting of the protein ovalbumin mixed with the adjuvant c-di-GMP, only immunization via the i.n. route induced ovalbumin-specific CD103-expressing CD8$^+$T cells in the BAL (Sup Fig. 2C,D). The subcutaneous route, like the i.m. route above, induced only CD103^{neg}CD49a$^+$CD8$^+$T cells (Fig. S2 C,D). These two T_{RM} populations expressed more granzyme B than effector T cells (Fig. S4 and data not shown). This difference was significant for the CD103$^+$CD49a$^+$ population.

Characterization of these resident memory E7-specific CD8$^+$ T cell subpopulations (CD103$^+$CD49a$^+$ and CD103^{neg}CD49a$^+$) revealed that the CD103$^+$CD49a$^+$CD8$^+$T cells expressed more PD-1 (Mean: 78.04% $\pm$ 9.65%) as compared to the CD103^{neg}CD49a$^+$ population (Mean 62.66% $\pm$ 8.14%) and the CD103^{neg}CD49a^{neg} effector CD8$^+$ T cell population (Mean: 47.46% $\pm$ 7.03%). (Fig. 1C). Interestingly, the resident memory CD8$^+$ T cell population co-expressing CD103 and CD49a appeared to be more functional after antigenic stimulation with a peptide derived from the E7 protein, secreting more IFNγ, TNFα, CCL4, and CCL5 (Fig. 1D) highlighting the more functional and protective phenotype of these cells.

2. Distinct subpopulations of T_{RM}-type $CD8^+$T lymphocytes co-exist among lung TILs.

TILs were obtained from 20 dissociated tumors from patients with NSCLC. The same T_{RM} subpopulations identified in mice ($CD103^+CD49a^+$ and $CD103^-CD49a^+$) were detected in humans, with the $CD103^+CD49a^+$ population being present at a higher frequency (Mean: 47% $\pm$ 22.52% of total CD8)(Fig. 2A). Nearly all of these T_{RM} exhibited an effector memory (EM) T cell phenotype ($CCR7^-CD45RA^-$) (Fig. S3). The two T_{RM} subpopulations expressed CD69 at a higher frequency (Mean $\%CD69^+$: 87.2% $\pm$ 6.9% in $CD103^+CD49a^+$ and 66.6% $\pm$ 12.8% in $CD103^{neg}CD49a^+$) as compared to the effector $CD8^+$T cell population ($CD103^{neg}CD49a^{neg}$; 33.8% $\pm$ 14.12%) (Fig. 2B). The $CD103^+CD49a^+$ cells expressed exhaustion markers (PD-1, Tim-3, CD39) and the proliferation marker Ki67 significantly more frequently (Fig. 2B). These data were confirmed through single-cell transcriptomic analyses of intratumoral $CD8^+$ T cells, revealing that the resident memory $CD103^+CD49a^+CD8^+$ T cells exhibited higher levels of exhaustion and proliferation marker expression relative to the $CD103^-CD49a^+CD8^+$ T cell population (Fig. S4).

We regard the $CD103^{neg}CD49a^+$ population as a T_{RM} population, as most of these cells express CD69, which is considered to be a T_{RM} marker (Kumar et al., 2017). They also express the transcription factors Hobit and Runx3, which are hallmarks of T_{RM}. However, in contrast to mice, these transcription factors are not enriched in human T_{RM} (Fig. S5) (Hombrink et al., 2016).

3. Relationship between the T_{RM} subpopulations in terms of differentiation.

Four fresh tumors were used to conduct single-cell transcriptomic analyses, revealing that, among all the patients, the five most frequent clonotypes (TRA or TRB) of the double positive T_{RM} $CD8^+$T cell subpopulation ($CD103^+CD49a^+$) were also present in the single positive T_{RM} $CD8^+$ T cell subpopulation ($CD103^{neg}CD49a^+$) as well as in the $CD103^{neg}CD49a^{neg}$ effector $CD8^+$ T cell population (Fig. 3A). These clonotypes were most amplified in the $CD103^+CD49a^+CD8^+$ T cells, followed by the $CD103^{neg}C49a^+CD8^+$T cell population and finally the $CD103^{neg}CD49a^{neg}$ $CD8^+$T cell population (Fig. 3B), suggesting possible differentiation and proliferation of effector $CD8^+$ T lymphocytes into the resident memory $CD103^{neg}CD49a^+CD8^+$ T cells and then into resident memory $CD103^+CD49a^+CD8^+$ T cells. Based on the Jaccard and the Morisita-horn dissimilarity indices (Fig. 3C and 3D, respectively), we found that for 3 out of 4 patients analyzed, closer repertoire composition and less dissimilarity (index close to 0) was observed between the $CD103^+CD49a^+$ and the $CD103^{neg}CD49a^+$ $CD8^+$T cell populations as compared to the $CD103^{neg}CD49a^{neg}$ population, reinforcing the relationship between the two T_{RM} populations. With respect to the trajectories of these three subpopulations, another argument supports a more terminal differentiation of the $CD103^+CD49a^+$ T_{RM} population since they express less TCF1 progenitor (Fig. Sup 6). Indeed, in mice, the % of cells expressing

TCF-1, a stemness marker, is lower (Mean 57.03% ± s.d. 6.37%) in the $CD103^{+}CD49a^{+}$ $CD8^{+}$T cell population, than in the $CD103^{neg}CD49a^{+}CD8^{+}$T cells (Mean 73.1% ± 5.45%) and in the $CD103^{neg}CD49a^{neg}$ effector $CD8^{+}$T populations (Mean 71.78% ± 9.45%)(Fig. S6). In humans, multiplex *in situ* immunofluorescence imaging revealed that the $CD103^{+}CD49a^{+}CD8^{+}$T cell population does not express TCF-1 (results not shown), as described previously (Wu, Madi et al., 2020).

4. Distribution and infiltration of lung tumors by resident memory $CD8^{+}$ T cell subpopulations.

In situ multiplex immunofluorescence labeling has enabled us to compare infiltration by different T_{RM} subpopulations either in the tumoural or stromal zone (Fig. 4A). We also included the TCF-1 marker when conducting this staining (Fig. 4A), as it is often considered a marker of stemness potentially associated with response to immunotherapy (Sade-Feldman, Yizhak et al., 2018). We observed a higher density of total $CD8^{+}$T cells, as well as all T_{RM} subpopulations, in the stroma compared to the tumor zone (Fig. 4B). In the tumor, the $CD103^{+}CD49a^{+}$ $CD8^{+}$ T_{RM} population was more frequently detected (Mean: 20 ± 62 cells/mm^2) as compared to the $CD103^{-}CD49a^{+}CD8^{+}$ T_{RM} population (Mean: 9 ± 11 cells/mm^2), but both populations were also present in the stroma at higher density (Mean: 119 ± 179 cells/mm^2 for $CD103^{+}CD49a^{+}$ $CD8^{+}$ T cells; Mean: 92 ± 84 cells/mm^2 for $CD103^{-}CD49a^{+}CD8^{+}$T cells)(Fig. 4B). The CD49a marker has also been reported to be expressed by endothelial cells (Aman & Margadant, 2023) (Fig. 4A). The $TCF\text{-}1^{+}CD8^{+}$T cell population also infiltrated the tumor microenvironment in these patients, but these cells were only found in the stroma (Mean: 11 ± 15 cells/mm^2) and not in the tumor nest. $CD103^{+}CD49a^{+}CD8^{+}$ T cells were not found to express TCF-1, but 13% of the $CD103^{-}CD49a^{+}CD8^{+}$ T cells expressed TCF-1 (Fig. 4B, C). TCF-1 expression was mainly observed in the stromally localized populations but not in the epithelial tumor islets (Fig. 4B, C).

5. The resident memory $CD103^{+}CD49a^{+}CD8^{+}$T cell population is the strongest predictor of clinical responses to anti-PD-1 immunotherapy.

Cox Proportional-Hazards univariate analysis showed that PD-L1 remained the most predictive biomarker of clinical response (HR = 3.06 [0.002-6.31], P = 0.002) in NSCLC patients undergoing second-line treatment with anti-PD-1(Fig. 5A). Interestingly, the population of T_{RM} $CD8^{+}$ T cells localized in the tumor co-expressing CD103 and CD49a markers was also a pre-treatment feature correlated (HR = 2.41 [1.26-4.62], P = 0.008) with clinical response (Fig. 5A), but this association did not remain true in the stroma (HR = 1.76 [0.092-3.39], P = 0.09). Intratumoural infiltration by $CD103^{+}CD49a^{+}CD8^{+}$T cells did not predict clinical response as defined by the RECIST criteria (data not shown).

In the same analysis, total $CD8^+$ T cells (HR = 2.00 [1.04-3.84], P = 0.037) and TCF-1-expressing $CD8^+$ T cells (HR = 2.11 [1.09-4.06], P = 0.025) also served as biomarkers associated with clinical response (Fig. 5A). In contrast, the resident memory $CD103^-$ $CD49a^+CD8^+$ T cell population, did not predict clinical response to immunotherapy (Fig. 5A) irrespective of its stromal or tumoral location (HR = 1.66 [0.87,3.17], P = 0.12 and HR = 1.70[0.89-3.22), P = 0.106, respectively)

These results were confirmed through Kaplan-Meier survival curve analyses and log-rank tests, confirming the relationships between survival and infiltration by $CD103^+CD49a^+$ $CD8^+$T cells, total CD8 and TCF-1^+CD8^+ T cells, well as the expression of PD-L1 by tumor cells (TCs) (Fig. 5B). In contrast, only PD-L1 expression by TCs and infiltration by TCF-1^+CD8^+ T cells were correlated with PFS (HR = 2.89 [1.52-5.5], P= 0.01 and HR = 1.84 [1.02-3.31], P = 0.043) in these immunotherapy-treated patients (Fig. S7A). This observation was made when comparing two groups of patients dichotomized using the median values for the parameters of interest. When we focused on extreme values using tertiles as cut-offs, the intratumoral $CD103^+CD49a^+$ $CD8^+$ cell population appeared to be also prognostic variable for PFS (HR =2.22[1.05-4.67], P = 0.036) (Fig. S7B).

ROC curve analyses of $CD103^+CD49a^+CD8^+$T cell infiltration yielded an AUC of 0.88 when predicting overall survival at 2 years, with this being the most robust predictor as compared to the other analyzed parameters (Fig. 5C). In a multivariate model, we found that the $CD103^+CD49a^+CD8^+$ T cell population remained predictive of survival when the model was adjusted for potential cofounders including PD-L1 expression and the infiltration of TCF-1^+CD8^+T cells (Table 1).

To confirm these results in a second cohort, we selected NSCLC patients with PD-L1 expression on >50% of TCs who underwent first-line anti-PD-1 treatment (n = 30) or second-line treatment (n = 6). We found that only intratumoral infiltration by $CD8^+$ T_{RM} cells co-expressing CD103 and CD49a was correlated with patient survival (HR = 2.77[1.13-6.75], P = 0.025) (Fig. 6A), confirming the results obtained in the discovery cohort. Kaplan-Meier curves and log-rank tests (P = 0.025) were used to analyze patients dichotomized based on median values (Fig. 6B). Tumor infiltration by the $CD8^+$ T_{RM} cell population co-expressing CD103 and CD49a was also the only population correlated with PFS when using this same approach to patient dichotomization (HR = 2.62[1.18-5.81], P = 0.018) (Fig. 6C).

DISCUSSION

In this study, we have shown that the intratumoral $CD8^+$ T_{RM} cell population co-expressing CD103 and CD49a was highly predictive of response to immunotherapy in two cohorts of lung cancer patients undergoing first- or second-line PD-1 blockade treatment. The predictive performance of this biomarker was also observed in a multivariate analysis. In contrast, the

population of $CD8^+T_{RM}$ cells expressing CD49a without CD103 was not associated with patient response to immunotherapy, irrespective of whether these cells were located in tumors or in the stroma. To the best of our knowledge, no study to date has analyzed the differential prognostic value of resident memory T cell subpopulations. In most reports, CD103 expression alone has been used to define T_{RM} populations. However, different T_{RM} subpopulations have been defined according to a core marker profile that also includes CD49a and CD69. Our $CD103^{neg}CD49a^+CD8^+$ T_{RM} population exhibits other T_{RM} characteristics such as CD69 expression, and expresses transcription factors (Runx3 and Hobit) associated with the T_{RM} lineage. Using single-cell analyses, other groups have identified T_{RM} subpopulations in lung cancer at different stages of differentiation that share certain properties with our two populations, but their differential prognostic role has not been reported (Banchereau et al., 2021, Guo, Zhang et al., 2018). Previous work in melanoma had shown that a gene signature corresponding to the $CD103^+CD49^+CD8^+T_{RM}$ cell population was correlated with better overall patient survival (Zitti et al., 2023). The more protective effects of intratumorally rather than stromally localized $CD103^+$ expressing T_{RM} observed in this study has also been reported previously in in patients with melanoma, NSCLC, and endometrial cancer (Corgnac et al., 2020, Djenidi et al., 2015, Koh, Kim et al., 2017, Wang, Milne et al., 2016, Workel, Komdeur et al., 2016).

To explain the positive relationship between the $CD103^+CD49a^+CD8^+$T cell population and overall survival, several hypotheses can be put forward. We have shown in mouse models that $CD103^+CD49a^+CD8^+$ T cells are more functional than $CD103^-CD49a^+CD8^+$ T cells, even though they express higher levels of inhibitory receptors such as PD-1 in both humans and mice. Other work has also shown that the $CD103^+$ T_{RM} population is superior to its $CD103^-$ counterparts in the production of IFN-γ and TNF-α (Lin, Zhang et al., 2020, Watanabe, Gehad et al., 2015). The $CD103^+CD49a^+CD8^+T_{RM}$ population in the epidermis has also been reported as being the most cytotoxic population (Cheuk et al., 2017).

It may seem paradoxical that the most exhausted population of T_{RM} coexpressing CD103 and CD49a is the most functional and associated with a better prognosis. While some studies correlate exhaustion with poor clinical outcomes (Datar, Sanmamed et al., 2019, Ma, Zheng et al., 2019, Mazzaschi, Madeddu et al., 2018, Sade-Feldman et al., 2018), others have defined a subpopulation of $CD103^+CD8^+T_{RM}$ cells that appear exhausted, but are also characterized by a proliferative signature and clonal expansion, as well as superior functionality, and are associated with good patient outcomes (Amsen, van Gisbergen et al., 2018, Bassez et al., 2021, Clarke, Panwar et al., 2019, Gueguen, Metoikidou et al., 2021, Hornburg, Desbois et al., 2021, Thommen, Koelzer et al., 2018). To explain these contradictory results, it is worth noting there are different stages of exhaustion that are not equivalent in terms of functionality (Giles, Globig et al., 2023), and certain markers of exhaustion may also, in some situations,

correspond to markers of activation (Cheuk et al., 2017). Furthermore, based on some reports, it is likely that the CD103$^+$CD49a$^+$CD8$^+$T cell population is enriched for tumor-specific T cells. Corgnac et al. have shown that this population exhibits enhanced proliferation and cytotoxicity towards autologous tumor cells and frequently displays the oligoclonal expansion of TCR-β clonotypes (Corgnac et al., 2020). We have also shown that this population expresses high levels of PD-1, which is a marker of tumor-reactive TILs in melanoma (Gros, Robbins et al., 2014). Finally, this CD103$^+$CD49a$^+$CD8$^+$T cell population expressed high levels of CD39 (Fig. 2). The CD103$^+$CD39$^+$ T cell population reportedly has a stronger reactivity against tumors relative to other CD8$^+$ T cell subpopulations (Duhen, Duhen et al., 2018, Simoni, Becht et al., 2018). In contrast, the CD103$^-$CD49a$^+$CD8$^+$T cell population may be associated with TILs that are not engaged with antigen (Melssen, Lindsay et al., 2021). Finally, the absence of CD103 in this CD103$^-$CD49a$^+$CD8$^+$T cell population may affect the persistence of this population in the tumor microenvironment and explain its less significant protective role (Mackay, Rahimpour et al., 2013). In addition, antibody blockade of CD103 or CD103 genetic deficiency results in a reduction in tumor-infiltrating T cells and accelerated tumor progression in mice (Malik, Byrne et al., 2017, Murray, Fuertes Marraco et al., 2016).

Our work shows that there is a relationship between the two CD103$^+$CD49a$^+$CD8$^+$ and CD103$^-$CD49a$^+$CD8$^+$T$_{RM}$ subpopulations, with the former appearing to be more differentiated than the latter. Indeed, these two populations share various TCRs that are amplified in the CD103$^+$CD49a$^+$CD8$^+$T cell population. In addition, the CD103$^-$CD49a$^+$CD8$^+$T cell population exhibits higher levels of TCF-1 expression, a surrogate for progenitor cells, relative to the CD103$^+$CD49a$^+$CD8$^+$T cell population. Other studies have reported common progenitor populations present in the blood that differentiate into distinct T$_{RM}$ subpopulations within tissues (Gueguen et al., 2021, Mackay et al., 2013). Furthermore, it has been shown that during T cell priming, CD49a expression is induced in the lymph node, whereas CD103 expression is acquired after T cell migration in the lung parenchyma and its expression kinetics are more delayed (Haddadi, Thanthrige-Don et al., 2017, Murray et al., 2016). T$_{RM}$ differentiation in the lung parenchyma depends on the interaction of the T$_{RM}$ progenitor population with a specific DC population expressing CXCL16 and membrane IL-15 (Di Pilato, Kfuri-Rubens et al., 2021). Interestingly, the TCF1-expressing progenitor T cell population has also been associated with response to immunotherapy in many cancers (Kurtulus, Madi et al., 2019, Miller, Sen et al., 2019, Philip & Schietinger, 2022, Sade-Feldman et al., 2018, Siddiqui, Schaeuble et al., 2019). We also found that these stromal TCF-1$^+$CD8$^+$T cells are able to predict responses to immunotherapy, although in a multivariate analysis, only the intratumoral CD103$^+$CD49a$^+$CD8 T$_{RM}$ population which does not express TCF-1 remained statistically significant as a predictor of this clinical response.

One of the limitations of this study analyzing and comparing the predictive value of subpopulations of T_{RM} as a parameter of response to immunotherapy is that it was performed against total CD8, TCF-1^{+} progenitor T cells, and PD-L1, but not against markers of spatial interactions between PD-1 and PD-L1 or PD-L1 and CD8. These emerging biomarkers have also been reported to predict response to immunotherapy in NSCLC (Ghiringhelli, Bibeau et al., 2023, Sanchez-Magraner, Gumuzio et al., 2023).

This work provides a better understanding of why the CD103^{-}CD49a^{+}CD8^{+}T_{RM} population induced after systemic vaccination does not inhibit tumor growth, in contrast to the CD103^{+}CD49a^{+}T cell population induced by i.n. immunization (Nizard et al., 2017). We have previously shown that anti-CD49a antibodies reverse the therapeutic effect of the nasally administered vaccines, but were unable to distinguish which subpopulation (CD103^{+} or CD103^{neg}) of T_{RM} expressing CD49a was targeted by the vaccine (Sandoval et al., 2013). Cell transfer experiments were inconclusive (Nizard et al., 2017, Sandoval et al., 2013). This strengthens the rationale for mucosal vaccination to induce this protective T_{RM} subpopulation coexpressing CD103 and CD49a.

In clinical practice, patients with lung cancer expressing >50% PD-L1 are treated with anti-PD-1 alone or in combination with chemotherapy. The quantification of the intratumoral T_{RM} subpopulation co-expressing CD103 and CD49a could help guide clinical decision-making when considering these different therapeutic options.

METHODS

Sex was not considered as a clinical variable in this study

Investigators have been blinded to the patient clinical outcome during the experiment

1. Patient sample collection

Two tumor collections from lung cancer patients were provided for this study: i) A colcheckpoint cohort which included tumor tissues from lung cancer patients treated with anti-PD-1 (pembrolizumab or nivolumab) at the Hôpital Europeen Georges Pompidou (HEGP), regardless of the therapeutic line (1st or 2nd line or beyond). Pre-therapeutic biopsies (less than 6 months before the start of immunotherapy) were preferred for most patients, but archival biopsies were also available for some patients. This collection started in June 2016. The clinical database was available for this cohort through a local data warehouse (Bastien Rance); ii) The CERTIM (Immunomodulatory Therapies Multidisciplinary Study group) collection was created in February 2015 by Pr F Goldwasser (Department of Medical Oncology, Hôpital Cochin) and is a collaborative French multidisciplinary network of physicians involved in oncology and research, based at the Cochin Hospital (Paris, France). For this study, it enrolled lung cancer patients treated with anti-PD-1 agents (nivolumab or pembrolizumab). At least one tumor

biopsy was available for each patient included in the CERTIM cohort with a varying length of time before the start of immunotherapy, as well as a clinical database for each patient.

From these 2 collections, we selected a discovery cohort of 57 lung cancer patients who underwent 2nd line treatment with anti-PD-1 and a validation cohort of 36 patients, 30 of whom underwent 1st line anti-PD-1 treatment and 6 of whom underwent 2nd line treatment, and for whom tumor tissue from lung localization was available to avoid bias due to localization to other sites.

Flow chart analyses for these cohorts are shown in Fig S1. Characteristics of these two cohorts are presented in Tables S1 and S2.

2. Experimental animals

Wild-type female C57BL/6J mice were purchased from Janvier Labs. Experiments were performed using mice 8-10 weeks of age. All mice were housed in an INSERM U970-PARCC animal facility under specific pathogen-free conditions. Experimental protocols were approved by the ethics committee of Université Paris Cité (CEEA 34; approval MESR29315) in accordance with European guidelines (EC2010/63).

3. Murine vaccination and sample preparation

STxB-E7 is a DC target-based vaccine chemically linked to the HPV16 $E7_{43-57}$ antigen as described previously (Karaki, Blanc et al., 2021). Anesthetized mice were immunized twice on day 0 and day 14 via intranasal (i.n.) or intramuscular (i.m,) vaccination using STxB-E7, with alpha-galactosylceramide (α-GalCer) as an adjuvant (Funakoshi, Tebu-bio France). On day 21, mice were sacrificed. Intravascular staining was performed to discriminate between tissue-localized and blood-borne cells as described by Anderson et al. (Anderson, Sung et al., 2012). Briefly, 5 µg of anti-CD8α APC-efluo780 (clone 53-6-7, eBioscience/Thermofisher) was injected intravenously (i.v.) 3 min prior to bronchoalveolar lavage fluid (BAL) and tissue collection. BAL was collected from anesthetized mice by flushing the lungs with PBS-EDTA (0.5 mM) via a cannula inserted into the trachea (5 washes x 1 mL).

Lungs were perfused with PBS-EDTA (0.5 mM) and digested in RPMI-1640 medium containing 1 mg/mL collagenase type IV (Life Technologies/ Thermofisher) and 30 µg/mL DNase I (Roche). Lung cells were dissociated using the GentleMACS (Miltenyi Biotec, France) lung programs 1 and 2, with gentle shaking for 30 min at 37°C between both steps. Then, the obtained single-cell suspensions were filtered through a 70-µm strainer, washed with PB containing 2% FBS, suspended in a 40% Percoll solution, layered over a 75% Percoll solution (Sigma-Aldrich), and centrifuged for 20 min at room temperature (RT) at 600 xg. Cells at the interface layer were collected and washed.

After FcR blocking with CD16/32 Ab (clone 93, ebioscience/Life Technologies), cells were first incubated for 30 min at RT with PE-conjugated H-2 D^b-$E7_{49–57}$ dextramers (Immudex, Bredevej 2A, 2830 Virum, Denmark). Then, cells were washed and stained for surface molecules for 20 min at 4°C in PBS-2%FCS containing anti-mouse CD8β BUV495 (clone YTS156, eBioscience), CD3 PercpCy5.5 (clone 145 2C11, eBioscience/Life Technologies), CD103 Pacific Blue (clone 2E7, Biolegend), CD49a APC or vioFITC (Miltenyi Biotec), and CD69 (clone H1.2F3, Biolegend). For intracellular staining, after surface staining, cells were permeabilized using the FoxP3/Transcription Factor staining buffer set (eBiosciences) according to the manufacturer's protocols, after which they were stained with an intracellular mAb specific for Tcf1 (clone FAB8224R, Biotechne). All the cells were labeled using the live/dead cell aqua blue viability dye (Life Technologies). Data acquisition was performed with a BD Fortessa X20 instrument (Becton Dickinson), and data from live single cells were analyzed using the FlowJo Software (Tree Star Inc.). Tissue-localized $CD8^+$T cells were defined as $CD3^+CD8\alpha^-CD8\beta^+$ cells. The adjuvant C-Di-GMP was purchased from InvivoGen (Toulouse, France).

4. Single-cell analyses

4.1 Cell sorting

Fresh human tumors were collected in Hank's Balanced Salt Solution (HBSS). After being mechanically dissociated with a scalpel, they were digested with DNAse I (30 IU/mL, Roche) and Collagenase D (1 mg/mL, Roche) at 37°C for one hour. Primary cells were then isolated by successive filtration with a 70 µm Falcon cell strainer (BD Falcon) and a 20 µm Falcon cell strainer (BD Falcon) and counted using a Malassez chamber. Obtained cells were then stained with the fixable viability stain FVS 520 (eBioscience), APC-conjugated anti-CD8α (Biolegend), and BV421-conjugated anti-NKP46 (Biolegend). NKP46 was used to eliminate natural killer cells from the analysis during sorting.

4.2 Single-cell capture and RNA sequencing

After sorting, $CD8^+$ T cells were processed with the Chromium Single-cell 5′ v2 Library Kit (10X Genomics) based on the manufacturer's instructions. A total of 5,000 cells were loaded per channel of the 10X Chromium Controller as previously described (Benhamouda, Sam et al., 2022). The instrument initially produces an emulsion of 100,000 droplets containing zero or one cell, a single bead coated with a single 16-nucleotide barcode common to all cyclic DNA (cDNA) generated from the same cell, a UMI (Unique Molecular Identifier) sequence of 10 nucleotides specific to each transcript, a sequencing primer (R1), a poly (dT) sequence and all the reagents necessary for cell lysis and RNA reverse transcription. The emulsion was then gently transferred to a plate and incubated at 53°C for 45 min for reverse transcription, followed by the lysis of the cells.

cDNA was then purified and amplified for 12 cycles and used for library preparation. Single-cell barcoded cDNA libraries were again amplified by PCR after the addition of adaptors. The final libraries were qualified and quantified using Bioanalyzer (Agilent) and Qubit (Invitrogen) instruments, pooled together, and sequenced on the Illumina HiSeq X platform. Cells were sequenced to obtain about 30,000 reads per cell.

4.3 Single-cell RNA sequencing data analysis

The raw deep sequencing data were processed using the 10X Genomics CellRanger software package (v 2.1. or 3.0.2) with the GRCh38-3.0.0 reference genome. Subsequent counts were analyzed using scShinyHub (https://github.com/baj12/scShinyHub) with the number of reads per cell being normalized by dividing by the total number of reads for a given cell and then log2(x+1) transformed and scaled with a factor of 1000. Cell selection was performed manually using scShinyHub.

5. T cell receptor (TCR) analyses

5.1 Data Source

The raw data used for this TCR repertoire analysis came from the 4 fresh lung tumors described above that were used for single-cell transcriptomic analyses.

5.2 Data pre-processing

Single-cell immune profiling raw data were processed using Cell Ranger (v 6.1.1) using –reference = vdj_GRCh38_alts_ensembl-5.0.0.

5.3 Overlap analysis

Jaccard and Morisita-Horn distances were used to assess the dissimilarity between repertoires (Valkiers, de Vrij et al., 2022). The Jaccard index is a measure of the intersection between two populations relative to the size of their union and is independent of relative abundances, whereas the Morisita-Horn index considers the relative abundance of species in the sample. Both indices vary between 0 (No dissimilarity) and 1 (complete dissimilarity). JSI and Morisita Horn distances were calculated using the vegan package (Oksanen J, Simpson G, Blanchet F, Kindt R, Legendre P, Minchin P, O'Hara R, Solymos P, Stevens M, Szoecs E, Wagner H, Barbour M, Bedward M, Bolker B, Borcard D, Carvalho G, Chirico M, De Caceres M, Durand S, Evangelista H, FitzJohn R, Friendly M, Furneaux B, Hannigan G, Hill M, Lahti L, McGlinn D, Ouellette M, Ribeiro Cunha E, Smith T, Stier A, Ter Braak C, Weedon J (2022). _vegan: Community Ecology Package_. R package version 2.6-4, <https://CRAN.R-project.org/package=vegan)

5.4 Statistical comparisons

R v4.2.3 (www.r-project.org) was used to conduct all statistical analyses. Figures were generated using the ggplot2 package (https://doi.org/10.1007/978-3-319-24277-4), with the exception of heatmaps, which were generated with the pheatmap package (Kolde, R. pheatmap: pretty heatmaps. https://cran.r-project.org/web/packages/pheatmap/index.html (2019). Both indices are presented as dissimilarity values and vary between 0 (no dissimilarity) and 1 (complete dissimilarity).

6. Data Availability

Single-cell RNA sequencing (scRNA-seq) data from 4 fresh lung cancer samples were uploaded to the NCBI Gene Expression Omnibus (GEO) archive platform (https://www.ncbi.nlm.nih.gov/geo/) under accession number GSE160243.

7. Flow cytometry analyses of TILs

Freshly resected lung tumors and adjacent healthy lung tissue samples obtained from the Institut Mutualiste Montsouris and the Hôpital Marie-Lannelongue were immediately cut into small fragments and digested for 40 min at 37°C using a tumor dissociation kit (Miltenyi Biotech). The dissociated samples were smashed on 100 µm cell strainers, washed, and red blood cell lysis was performed. The recovered single-cell suspension was used for phenotypic analyses performed by direct immunofluorescence with a panel of fluorochrome-conjugated antibodies. Anti-CD3-Alexa700 (UCHT1), anti-CD8-PacificBlue (RPA-T8), anti-CD69-APC-Cy7 (FN50), anti-granzyme-B-FITC (GB11) were supplied by BioLegend. Anti-CD103-BV711 (Ber-ACT8) and anti-Hobit-Alexa647 (Sanquin-Hobit/1) were purchased from BD Biosciences. Anti-CD49-PerCPefluor710 (TS2/7) and anti-PD-1-PeCy7 (eBioJ105) were supplied by Thermo Fisher Scientific. Anti-RUNX3-PE (R3-5G4) and CCR7-PeCy7 (3D12) were purchased from BD Pharmingen. Anti-CD45RA-APC and anti-CD39-APC, were purchased from Miltenyi. Cells were fixed, permeabilized (FoxP3 Buffer Kit, eBioscience) and then stained with fluorochrome-conjugated mAbs. Dead cells were excluded using a LIVE/DEAD Fixable UV dead cell stain kit (Thermo Fisher Scientific). Stained cells were analyzed by flow cytometry using a BD FACS Fortessa flow cytometer (BD Biosciences). Data were processed using FlowJo software (Tree Star Inc..) (Corgnac, Lecluse et al., 2021). This study was approved by the Institutional Review Board of Gustave Roussy (Commission scientifique des Essais thérapeutiques [CSET]) and informed consent was obtained.

8. Multiplex immunofluorescence staining

T_{RM} cell infiltration was assessed using formalin-fixed paraffin-embedded (FFPE) slides (4 µM-thick sections) stained with a panel that had been developed manually before being automated

with a Leica Bond robot (Leica Biosystems, Wetzlar, Germany). Slides were deparaffinized (Bond Dewax Solution, Leica Biosystems) and then rehydrated via immersion in decreasing concentrations of ethanol in distilled water. Slides were then fixed in 4% paraformaldehyde. Heating mediated-epitope/antigen retrieval was performed with Bond TM Epitope Retrieval 2 (Leica Biosystems). Blocking was performed with plant-based protein blocking buffer (Cell Signaling Technology [CST], MA, USA) for 15 min. Primary mAbs directed against selected antigens were diluted in SignalStain® Antibody Diluent (CST) and incubated for 30 min (except for CD49a, 60 min). Secondary antibodies conjugated to horseradish peroxidase (ImmunoReagents, NC, USA) were then incubated on samples for 15 minutes (except for CD49a, 45 min). Finally, immunofluorescence labeling was performed with the CF® Dye Tyramide from Biotium (CA, USA). The slides were then washed and heated to remove non-adsorbed antibodies/dye, followed by saturation, labeling with the primary and secondary antibodies, repeating this as many times as necessary to achieve multiplexed labeling. The specificity of each antibody was validated using an isotype control.

The list of antibodies and reagents is provided in Table S3. After the final labeling, samples were stained with DAPI for nuclear counterstaining (PerkinElmer, MA, USA) and mounted in EverBrite Mounting Medium (Biotium).

9. Multispectral imaging and phenotyping

Biopsies were whole-slide scanned using the Vectra System (PerkinElmer) at 20x magnification. Ten regions of interest were then selected using Phenochart whole-slide reviewer (PerkinElmer). A spectral library enabling the unmixing of dye was prepared using unstained and single-stained tonsil tissues. The inForm Cell Analysis software (PerkinElmer) was used to facilitate cell segmentation and phenotyping based in part on DAPI staining. A phenotyping step was then performed by training the software to recognize cells depending on their expressed surface biomarkers in order to define an analytical algorithm. Cells were then manually checked until the automatized recognition by InForm® was consistent with the visual count. Each phenotype image was checked after software analysis. The InForm® software provides a confidence interval for each phenotyped cell. For the final statistical analysis, cells were taken into account only if the given confidence interval was over 55% for the corresponding phenotype. The data was then analyzed using R software and the phenoptrReports package (Akoya).

10. *In vitro* stimulation and multiplex cytokine assay

Single-cell preparations were obtained from the BAL and lungs of mice on day 21 after i.n vaccination as described previously. Total $CD8^+$ T cells were isolated by magnetic sorting (EasySep™ Mouse $CD8^+$ T Cell Isolation Kit, StemCell Technologies), followed by tetramer E7

and T_{RM} marker staining. Then, E7-specific T_{RM} $CD103^{+}CD49a^{+}$, $CD103^{neg}CD49a^{+}$, and Teff $CD103^{neg}CD49a^{neg}$ populations were sorted by flow cytometry and stimulated (10,000 cells/well) with $E7_{49-57}$ peptide (10 µg/mL) for 18 h. Then, supernatants were harvested and a bead-based multiplexed cytokine immunoassay was performed to detect IL-2, IFNγ, Granzyme B, MIP1a/CCL3, MIP1b/CCL4, and RANTES/CCL5 (R&D Biotechne) according to the manufacturer's protocol and analyzed using the Bio-Plex 200 platform (Bio-rad). Analyte concentrations were calculated using a standard curve (5 PL regression) with the Bio-Plex manager software.

11. Statistical analysis

All statistical analyses were performed using R v 3.4.2. Kaplan–Meier curves (to visualize survival probabilities) and Log-rank tests (to test for statistical significance between groups) were performed using the ggsurvplot function of the survimer package. Univariate analyses for both overall survival (OS) and progression-free survival (PFS) were conducted using a Cox Proportional Hazards model implemented in the coxph function of the survival package, retrieving hazard ratios (HRs), 95% confidence intervals, and Wald statistics to address the statistical significance of the model. For each variable of interest, the data were dichotomized into "Low" and 'High" groups according to the median or extreme tertile cut-offs of the distribution for the univariate survival analysis.

Time-dependent receiver operating characteristic (ROC) curve and AUC (area under the curve) analyses were conducted with the survivalROC package configured using the Nearest Neighbor Estimation (NNE) method. The Cox proportional hazard model was also used to perform a multivariate analysis to assess whether the prognostic effect of a variable of interest remains significant after adjustment for other potential cofounders. These variables were considered as continuous variables whereas the variable of interest was dichotomized into two groups.

12.Study Approval

All clinical investigation have been conducted according to Declaration of Helsinki principles

Written informed consent was received from participants prior to inclusion in the study.

The colcheckpoint cohort has received the approval of the CPP Ile de France II (CPP number : 2015-08-04-MS2) and the CNIL declaration (iDP1563364). For the Certim cohort protocol was approved by the local ethics committee (CPP Ile de France II, n°2008-133 and 2012 06-12, MS1) in accordance with article L.1121-1 of the French law.

Acknowledgments

This work was funded by the Fondation ARC pour la Recherche sur le Cancer (Grant number SIGN'IT20181007747 and PGA 2020 12019110000946_1581 to E. Tartour), the INCA (Institut National du Cancer) (Grant number 2022 PLBIO22-147 to E. Tartour), PCSI 2021 (M2DIA), the Agence Nationale de la Recherche (Labex Immuno-Oncology to E. Tartour), the Institut National du Cancer (Grant SIRIC CARPEM to E. Tartour, L Paolini, S. Oudard), FONCER (to E. Tartour), Fondation pour la Recherche Médicale (FRM) (EQU202103012926 to Ludger Johannes), Institut National du Cancer (INCa) (contract n°2019-1-PLBIO-05-1 to Eric Tartour and Ludger Johannes), La Ligue MucoRNAvax (Convention N°AAPARN 2021.LCC/ChP to Eric Tartour and Ludger Johannes), PEPR RNAvac (ANR-22-PEBI-0007 to Eric Tartour and Ludger Johannes)

We thank the staff of the tumour banks of HEGP (B. Vedie and D. Geromin) for providing the sample materials and the Histology platform of PARCC (C. Lesaffre).

Conflict of Interest

None

The Paper Explained

PROBLEM

Tumor infiltration by resident memory T-CD8 lymphocytes (T_{RM}) is often associated with response to immunotherapy, but its predictive value has not yet led to its recommendation in patient management guidelines. There are different sub-populations of T_{RM} whose specific role is not well understood.

RESULTS

We identified two main T_{RM} subpopulations in tumor-infiltrating lymphocytes derived from non-small cell lung cancer (NSCLC) patients: one co-expressing CD103 and CD49a (DP), and the other expressing only CD49a (MP); both exhibiting additional T_{RM} surface markers like CD69. DP T_{RM} exhibited greater functionality compared to MP T_{RM}. Analysis of T-cell receptor (TCR) repertoire and of the stemness marker TCF-1 revealed shared TCRs between populations, with the MP subset appearing more progenitor-like phenotype. In two NSCLC patient cohorts, only DP T_{RM} predicted PD-1 blockade response. Multivariate analysis, including various biomarkers (CD8, $TCF1^+CD8^+$T cells, and PD-L1) associated with responses to anti-PD(L)1, showed that only intra-tumoral infiltration by DP T_{RM} remained significant

IMPACT

This work shows that it is crucial to distinguish between T_{RM} subpopulations because they have different functionalities, and only the intratumoral T_{RM} population expressing CD103 and CD49a can effectively predict the clinical response of non-small cell lung cancers to immunotherapy.

Author contributions

LP and TT contributed to the conception of the work, acquisition, analysis, interpretation of the data, and drafting of the manuscript. ET carried out the coordination of the work.
SC conducted experiments, acquired, analyzed and interpreted the data and drafted the manuscript
DD contributed to the conception of the work, analyzed and interpreted the data and drafted the manuscript
JPV, MW, JA contributed to the analysis, and interpretation of the data, as well as critically reviewing the manuscript.
JP, AG, VQ, PB, MH, VL, SM conducted experiments and contributed to analysis and interpretation of the data and review it critically.
LJ, JU, LVV, NG, SdP, PB-R, FG, IC, KL, PLP, HdSB, LG, PR,FMC, EF contributed to analysis and interpretation of the data and review it critically.
All authors participated in final approval of the version to be published.

References

Aman J, Margadant C (2023) Integrin-Dependent Cell-Matrix Adhesion in Endothelial Health and Disease. *Circ Res* 132: 355-378

Amsen D, van Gisbergen K, Hombrink P, van Lier RAW (2018) Tissue-resident memory T cells at the center of immunity to solid tumors. *Nat Immunol* 19: 538-546

Anderson KG, Sung H, Skon CN, Lefrancois L, Deisinger A, Vezys V, Masopust D (2012) Cutting edge: intravascular staining redefines lung CD8 T cell responses. *J Immunol* 189: 2702-6

Ariotti S, Hogenbirk MA, Dijkgraaf FE, Visser LL, Hoekstra ME, Song JY, Jacobs H, Haanen JB, Schumacher TN (2014) T cell memory. Skin-resident memory CD8(+) T cells trigger a state of tissue-wide pathogen alert. *Science* 346: 101-5

Attrill GH, Owen CN, Ahmed T, Vergara IA, Colebatch AJ, Conway JW, Nahar KJ, Thompson JF, Pires da Silva I, Carlino MS, Menzies AM, Lo S, Palendira U, Scolyer RA, Long GV, Wilmott JS (2022) Higher proportions of CD39+ tumor-resident cytotoxic T cells predict recurrence-free survival in patients with stage III melanoma treated with adjuvant immunotherapy. *J Immunother Cancer* 10

Banchereau R, Chitre AS, Scherl A, Wu TD, Patil NS, de Almeida P, Kadel Iii EE, Madireddi S, Au-Yeung A, Takahashi C, Chen YJ, Modrusan Z, McBride J, Nersesian R, El-Gabry EA, Robida MD, Hung JC, Kowanetz M, Zou W, McCleland M et al. (2021) Intratumoral CD103+ CD8+ T cells predict response to PD-L1 blockade. *J Immunother Cancer* 9

Bassez A, Vos H, Van Dyck L, Floris G, Arijs I, Desmedt C, Boeckx B, Vanden Bempt M, Nevelsteen I, Lambein K, Punie K, Neven P, Garg AD, Wildiers H, Qian J, Smeets A, Lambrechts D (2021) A single-cell map of intratumoral changes during anti-PD1 treatment of patients with breast cancer. *Nat Med* 27: 820-832

Benhamouda N, Sam I, Epaillard N, Gey A, Phan L, Pham HP, Gruel N, Saldmann A, Pineau J, Hasan M, Quiniou V, Nevoret C, Verkarre V, Libri V, Mella S, Granier C, Broudin C, Ravel P, De Guillebon E, Mauge L et al. (2022) Plasma CD27, a Surrogate of the Intratumoral CD27-CD70 Interaction, Correlates with Immunotherapy Resistance in Renal Cell Carcinoma. *Clin Cancer Res* 28: 4983-4994

Bergsbaken T, Bevan MJ (2015) Proinflammatory microenvironments within the intestine regulate the differentiation of tissue-resident CD8(+) T cells responding to infection. *Nat Immunol* 16: 406-14

Cheuk S, Schlums H, Gallais Serezal I, Martini E, Chiang SC, Marquardt N, Gibbs A, Detlofsson E, Introini A, Forkel M, Hoog C, Tjernlund A, Michaelsson J, Folkersen L, Mjosberg J, Blomqvist L, Ehrstrom M, Stahle M, Bryceson YT, Eidsmo L (2017) CD49a Expression Defines Tissue-Resident CD8(+) T Cells Poised for Cytotoxic Function in Human Skin. *Immunity* 46: 287-300

Clarke J, Panwar B, Madrigal A, Singh D, Gujar R, Wood O, Chee SJ, Eschweiler S, King EV, Awad AS, Hanley CJ, McCann KJ, Bhattacharyya S, Woo E, Alzetani A, Seumois G, Thomas GJ, Ganesan AP, Friedmann PS, Sanchez-Elsner T et al. (2019) Single-cell transcriptomic analysis of tissue-resident memory T cells in human lung cancer. *J Exp Med* 216: 2128-2149

Corgnac S, Lecluse Y, Mami-Chouaib F (2021) Isolation of tumor-resident CD8(+) T cells from human lung tumors. *STAR Protoc* 2: 100267

Corgnac S, Malenica I, Mezquita L, Auclin E, Voilin E, Kacher J, Halse H, Grynszpan L, Signolle N, Dayris T, Leclerc M, Droin N, de Montpreville V, Mercier O, Validire P, Scoazec JY, Massard C, Chouaib S, Planchard D, Adam J et al. (2020) CD103(+)CD8(+) TRM Cells Accumulate in Tumors of Anti-PD-1-Responder Lung Cancer Patients and Are Tumor-Reactive Lymphocytes Enriched with Tc17. *Cell Rep Med* 1: 100127

Datar I, Sanmamed MF, Wang J, Henick BS, Choi J, Badri T, Dong W, Mani N, Toki M, Mejias LD, Lozano MD, Perez-Gracia JL, Velcheti V, Hellmann MD, Gainor JF, McEachern K, Jenkins D, Syrigos K, Politi K, Gettinger S et al. (2019) Expression Analysis and Significance of PD-1, LAG-3, and TIM-3 in Human Non-Small Cell Lung Cancer Using Spatially Resolved and Multiparametric Single-Cell Analysis. *Clin Cancer Res* 25: 4663-4673

Di Pilato M, Kfuri-Rubens R, Pruessmann JN, Ozga AJ, Messemaker M, Cadilha BL, Sivakumar R, Cianciaruso C, Warner RD, Marangoni F, Carrizosa E, Lesch S, Billingsley J, Perez-Ramos D, Zavala F, Rheinbay E, Luster AD, Gerner MY, Kobold S, Pittet MJ et al. (2021) CXCR6 positions cytotoxic T cells to receive critical survival signals in the tumor microenvironment. *Cell* 184: 4512-4530 e22

Djenidi F, Adam J, Goubar A, Durgeau A, Meurice G, de Montpreville V, Validire P, Besse B, Mami-Chouaib F (2015) CD8+CD103+ tumor-infiltrating lymphocytes are tumor-specific tissue-resident memory T cells and a prognostic factor for survival in lung cancer patients. *J Immunol* 194: 3475-86

Douguet L, Fert I, Lopez J, Vesin B, Le Chevalier F, Moncoq F, Authie P, Nguyen TM, Noirat A, Nevo F, Blanc C, Bourgine M, Hardy D, Anna F, Majlessi L, Charneau P (2023) Full eradication of pre-clinical human papilloma virus-induced tumors by a lentiviral vaccine. *EMBO Mol Med*: e17723

Duhen T, Duhen R, Montler R, Moses J, Moudgil T, de Miranda NF, Goodall CP, Blair TC, Fox BA, McDermott JE, Chang SC, Grunkemeier G, Leidner R, Bell RB, Weinberg AD (2018) Co-expression of CD39 and CD103 identifies tumor-reactive CD8 T cells in human solid tumors. *Nat Commun* 9: 2724

Edwards J, Wilmott JS, Madore J, Gide TN, Quek C, Tasker A, Ferguson A, Chen J, Hewavisenti R, Hersey P, Gebhardt T, Weninger W, Britton WJ, Saw RPM, Thompson JF, Menzies AM, Long GV, Scolyer RA, Palendira U (2018) CD103(+) Tumor-Resident CD8(+) T Cells Are Associated with Improved Survival in Immunotherapy-Naive Melanoma Patients and Expand Significantly During Anti-PD-1 Treatment. *Clin Cancer Res* 24: 3036-3045

Ganesan AP, Clarke J, Wood O, Garrido-Martin EM, Chee SJ, Mellows T, Samaniego-Castruita D, Singh D, Seumois G, Alzetani A, Woo E, Friedmann PS, King EV, Thomas GJ, Sanchez-Elsner T, Vijayanand P, Ottensmeier CH (2017) Tissue-resident memory features are linked to the magnitude of cytotoxic T cell responses in human lung cancer. *Nat Immunol* 18: 940-950

Ge C, Monk IR, Pizzolla A, Wang N, Bedford JG, Stinear TP, Westall GP, Wakim LM (2019) Bystander Activation of Pulmonary Trm Cells Attenuates the Severity of Bacterial Pneumonia by Enhancing Neutrophil Recruitment. *Cell Rep* 29: 4236-4244 e3

Ghiringhelli F, Bibeau F, Greillier L, Fumet JD, Ilie A, Monville F, Lauge C, Catteau A, Boquet I, Majdi A, Morgand E, Oulkhouir Y, Brandone N, Adam J, Sbarrato T, Kassambara A, Fieschi J, Garcia S, Lepage AL, Tomasini P et al. (2023) Immunoscore immune checkpoint using spatial quantitative analysis of CD8 and PD-L1 markers is predictive of the efficacy of anti- PD1/PD-L1 immunotherapy in non-small cell lung cancer. *EBioMedicine* 92: 104633

Giles JR, Globig AM, Kaech SM, Wherry EJ (2023) CD8(+) T cells in the cancer-immunity cycle. *Immunity* 56: 2231-2253

Gros A, Robbins PF, Yao X, Li YF, Turcotte S, Tran E, Wunderlich JR, Mixon A, Farid S, Dudley ME, Hanada K, Almeida JR, Darko S, Douek DC, Yang JC, Rosenberg SA (2014) PD-1 identifies the patient-specific CD8(+) tumor-reactive repertoire infiltrating human tumors. *J Clin Invest* 124: 2246-59

Gueguen P, Metoikidou C, Dupic T, Lawand M, Goudot C, Baulande S, Lameiras S, Lantz O, Girard N, Seguin-Givelet A, Lefevre M, Mora T, Walczak AM, Waterfall JJ, Amigorena S (2021) Contribution of resident and circulating precursors to tumor-infiltrating CD8(+) T cell populations in lung cancer. *Sci Immunol* 6

Guo X, Zhang Y, Zheng L, Zheng C, Song J, Zhang Q, Kang B, Liu Z, Jin L, Xing R, Gao R, Zhang L, Dong M, Hu X, Ren X, Kirchhoff D, Roider HG, Yan T, Zhang Z (2018) Global characterization of T cells in non-small-cell lung cancer by single-cell sequencing. *Nat Med* 24: 978-985

Haddadi S, Thanthrige-Don N, Afkhami S, Khera A, Jeyanathan M, Xing Z (2017) Expression and role of VLA-1 in resident memory CD8 T cell responses to respiratory mucosal viral-vectored immunization against tuberculosis. *Sci Rep* 7: 9525

Hombrink P, Helbig C, Backer RA, Piet B, Oja AE, Stark R, Brasser G, Jongejan A, Jonkers RE, Nota B, Basak O, Clevers HC, Moerland PD, Amsen D, van Lier RA (2016) Programs for the persistence, vigilance and control of human CD8+ lung-resident memory T cells. *Nat Immunol* 17: 1467-1478

Hornburg M, Desbois M, Lu S, Guan Y, Lo AA, Kaufman S, Elrod A, Lotstein A, DesRochers TM, Munoz-Rodriguez JL, Wang X, Giltnane J, Mayba O, Turley SJ, Bourgon R, Daemen A, Wang Y (2021) Single-cell dissection of cellular components and interactions shaping the tumor immune phenotypes in ovarian cancer. *Cancer Cell* 39: 928-944 e6

Iijima N, Iwasaki A (2014) T cell memory. A local macrophage chemokine network sustains protective tissue-resident memory CD4 T cells. *Science* 346: 93-8

Jaiswal A, Verma A, Dannenfelser R, Melssen M, Tirosh I, Izar B, Kim TG, Nirschl CJ, Devi KSP, Olson WC, Jr., Slingluff CL, Jr., Engelhard VH, Garraway L, Regev A, Minkis K, Yoon CH, Troyanskaya O, Elemento O, Suarez-Farinas M, Anandasabapathy N (2022) An activation to memory differentiation trajectory of tumor-infiltrating lymphocytes informs metastatic melanoma outcomes. *Cancer Cell* 40: 524-544 e5

Jeyanathan M, Fritz DK, Afkhami S, Aguirre E, Howie KJ, Zganiacz A, Dvorkin-Gheva A, Thompson MR, Silver RF, Cusack RP, Lichty BD, O'Byrne PM, Kolb M, Medina MFC, Dolovich MB, Satia I, Gauvreau GM, Xing Z, Smaill F (2022) Aerosol delivery, but not intramuscular injection, of adenovirus-vectored tuberculosis vaccine induces respiratory-mucosal immunity in humans. *JCI Insight* 7

Karaki S, Blanc C, Tran T, Galy-Fauroux I, Mougel A, Dransart E, Anson M, Tanchot C, Paolini L, Gruel N, Gibault L, Lepimpec-Barhes F, Fabre E, Benhamouda N, Badoual C, Damotte D, Donnadieu E, Kobold S, Mami-Chouaib F, Golub R et al. (2021) CXCR6 deficiency impairs cancer vaccine efficacy and CD8(+) resident memory T-cell recruitment in head and neck and lung tumors. *J Immunother Cancer* 9: e001948

Koh J, Kim S, Kim MY, Go H, Jeon YK, Chung DH (2017) Prognostic implications of intratumoral CD103+ tumor-infiltrating lymphocytes in pulmonary squamous cell carcinoma. *Oncotarget* 8: 13762-13769

Kumar BV, Ma W, Miron M, Granot T, Guyer RS, Carpenter DJ, Senda T, Sun X, Ho SH, Lerner H, Friedman AL, Shen Y, Farber DL (2017) Human Tissue-Resident Memory T Cells Are Defined by Core Transcriptional and Functional Signatures in Lymphoid and Mucosal Sites. *Cell Rep* 20: 2921-2934

Kunzli M, O'Flanagan SD, LaRue M, Talukder P, Dileepan T, Stolley JM, Soerens AG, Quarnstrom CF, Wijeyesinghe S, Ye Y, McPartlan JS, Mitchell JS, Mandl CW, Vile R, Jenkins MK, Ahmed R, Vezys V, Chahal JS, Masopust D (2022) Route of self-amplifying mRNA vaccination modulates the establishment of pulmonary resident memory CD8 and CD4 T cells. *Sci Immunol* 7: eadd3075

Kurtulus S, Madi A, Escobar G, Klapholz M, Nyman J, Christian E, Pawlak M, Dionne D, Xia J, Rozenblatt-Rosen O, Kuchroo VK, Regev A, Anderson AC (2019) Checkpoint Blockade Immunotherapy Induces Dynamic Changes in PD-1(-)CD8(+) Tumor-Infiltrating T Cells. *Immunity* 50: 181-194 e6

Lin R, Zhang H, Yuan Y, He Q, Zhou J, Li S, Sun Y, Li DY, Qiu HB, Wang W, Zhuang Z, Chen B, Huang Y, Liu C, Wang Y, Cai S, Ke Z, He W (2020) Fatty Acid Oxidation Controls CD8(+) Tissue-Resident Memory T-cell Survival in Gastric Adenocarcinoma. *Cancer Immunol Res* 8: 479-492

Luoma AM, Suo S, Wang Y, Gunasti L, Porter CBM, Nabilsi N, Tadros J, Ferretti AP, Liao S, Gurer C, Chen YH, Criscitiello S, Ricker CA, Dionne D, Rozenblatt-Rosen O, Uppaluri R, Haddad RI, Ashenberg O, Regev A, Van Allen EM et al. (2022) Tissue-resident memory and circulating T cells are early responders to pre-surgical cancer immunotherapy. *Cell* 185: 2918-2935 e29

Ma J, Zheng B, Goswami S, Meng L, Zhang D, Cao C, Li T, Zhu F, Ma L, Zhang Z, Zhang S, Duan M, Chen Q, Gao Q, Zhang X (2019) PD1(Hi) CD8(+) T cells correlate with exhausted signature and poor clinical outcome in hepatocellular carcinoma. *J Immunother Cancer* 7: 331

Mackay LK, Rahimpour A, Ma JZ, Collins N, Stock AT, Hafon ML, Vega-Ramos J, Lauzurica P, Mueller SN, Stefanovic T, Tscharke DC, Heath WR, Inouye M, Carbone FR, Gebhardt T (2013) The developmental pathway for CD103(+)CD8+ tissue-resident memory T cells of skin. *Nat Immunol* 14: 1294-301

Malik BT, Byrne KT, Vella JL, Zhang P, Shabaneh TB, Steinberg SM, Molodtsov AK, Bowers JS, Angeles CV, Paulos CM, Huang YH, Turk MJ (2017) Resident memory T cells in the skin mediate durable immunity to melanoma. *Sci Immunol* 2

Mami-Chouaib F, Blanc C, Corgnac S, Hans S, Malenica I, Granier C, Tihy I, Tartour E (2018) Resident memory T cells, critical components in tumor immunology. *J Immunother Cancer* 6: 87

Masopust D, Vezys V, Marzo AL, Lefrancois L (2001) Preferential localization of effector memory cells in nonlymphoid tissue. *Science* 291: 2413-7.

Mazzaschi G, Madeddu D, Falco A, Bocchialini G, Goldoni M, Sogni F, Armani G, Lagrasta CA, Lorusso B, Mangiaracina C, Vilella R, Frati C, Alfieri R, Ampollini L, Veneziani M, Silini EM, Ardizzoni A, Urbanek K, Aversa F, Quaini F et al. (2018) Low PD-1 Expression in Cytotoxic CD8(+) Tumor-Infiltrating Lymphocytes Confers an Immune-Privileged Tissue Microenvironment in NSCLC with a Prognostic and Predictive Value. *Clin Cancer Res* 24: 407-419

Melssen MM, Lindsay RS, Stasiak K, Rodriguez AB, Briegel AM, Cyranowski S, Rutkowski MR, Conaway MR, Melief CJM, van der Burg SH, Eyo U, Slingluff CL, Jr., Engelhard VH (2021) Differential Expression of CD49a and CD49b Determines Localization and Function of Tumor-Infiltrating CD8(+) T Cells. *Cancer Immunol Res* 9: 583-597

Menares E, Galvez-Cancino F, Caceres-Morgado P, Ghorani E, Lopez E, Diaz X, Saavedra-Almarza J, Figueroa DA, Roa E, Quezada SA, Lladser A (2019) Tissue-resident memory CD8(+) T cells amplify anti-tumor immunity by triggering antigen spreading through dendritic cells. *Nat Commun* 10: 4401

Miller BC, Sen DR, Al Abosy R, Bi K, Virkud YV, LaFleur MW, Yates KB, Lako A, Felt K, Naik GS, Manos M, Gjini E, Kuchroo JR, Ishizuka JJ, Collier JL, Griffin GK, Maleri S, Comstock DE, Weiss SA, Brown FD et al. (2019) Subsets of exhausted CD8(+) T cells differentially mediate tumor control and respond to checkpoint blockade. *Nat Immunol* 20: 326-336

Murray T, Fuertes Marraco SA, Baumgaertner P, Bordry N, Cagnon L, Donda A, Romero P, Verdeil G, Speiser DE (2016) Very Late Antigen-1 Marks Functional Tumor-Resident CD8 T Cells and Correlates with Survival of Melanoma Patients. *Front Immunol* 7: 573

Nizard M, Roussel H, Diniz MO, Karaki S, Tran T, Voron T, Dransart E, Sandoval F, Riquet M, Rance B, Marcheteau E, Fabre E, Mandavit M, Terme M, Blanc C, Escudie JB, Gibault L, Barthes FLP, Granier C, Ferreira LCS et al. (2017) Induction of resident memory T cells enhances the efficacy of cancer vaccine. *Nat Commun* 8: 15221

Okla K, Farber DL, Zou W (2021) Tissue-resident memory T cells in tumor immunity and immunotherapy. *J Exp Med* 218

Philip M, Schietinger A (2022) CD8(+) T cell differentiation and dysfunction in cancer. *Nat Rev Immunol* 22: 209-223

Sade-Feldman M, Yizhak K, Bjorgaard SL, Ray JP, de Boer CG, Jenkins RW, Lieb DJ, Chen JH, Frederick DT, Barzily-Rokni M, Freeman SS, Reuben A, Hoover PJ, Villani AC, Ivanova E, Portell A, Lizotte PH, Aref AR, Eliane JP, Hammond MR et al. (2018) Defining T Cell States Associated with Response to Checkpoint Immunotherapy in Melanoma. *Cell* 175: 998-1013 e20

Sanchez-Magraner L, Gumuzio J, Miles J, Quimi N, Martinez Del Prado P, Abad-Villar MT, Pikabea F, Ortega L, Etxezarraga C, Martin-Algarra S, Lozano MD, Saiz-Camin M, Egurrola-Izquierdo M, Barredo-Santamaria I, Saiz-Lopez A, Gomez-Mediavilla J, Segues-Merino N, Juaristi-Abaunz MA, Urruticoechea A, Geraedts EJ et al. (2023) Functional Engagement of the PD-1/PD-L1 Complex But Not PD-L1 Expression Is Highly Predictive of Patient Response to Immunotherapy in Non-Small-Cell Lung Cancer. *J Clin Oncol* 41: 2561-2570

Sandoval F, Terme M, Nizard M, Badoual C, Bureau MF, Freyburger L, Clement O, Marcheteau E, Gey A, Fraisse G, Bouguin C, Merillon N, Dransart E, Tran T, Quintin-Colonna F, Autret G, Thiebaud M, Suleman M, Riffault S, Wu TC et al. (2013) Mucosal Imprinting of Vaccine-Induced CD8+ T Cells Is Crucial to Inhibit the Growth of Mucosal Tumors. *Sci Transl Med* 5: 172ra20

Schenkel JM, Fraser KA, Masopust D (2014) Cutting edge: resident memory CD8 T cells occupy frontline niches in secondary lymphoid organs. *J Immunol* 192: 2961-4

Schenkel JM, Masopust D (2014) Tissue-resident memory T cells. *Immunity* 41: 886-97

Siddiqui I, Schaeuble K, Chennupati V, Fuertes Marraco SA, Calderon-Copete S, Pais Ferreira D, Carmona SJ, Scarpellino L, Gfeller D, Pradervand S, Luther SA, Speiser DE, Held W (2019) Intratumoral Tcf1(+)PD-1(+)CD8(+) T Cells with Stem-like Properties Promote Tumor Control in Response to Vaccination and Checkpoint Blockade Immunotherapy. *Immunity* 50: 195-211 e10

Simoni Y, Becht E, Fehlings M, Loh CY, Koo SL, Teng KWW, Yeong JPS, Nahar R, Zhang T, Kared H, Duan K, Ang N, Poidinger M, Lee YY, Larbi A, Khng AJ, Tan E, Fu C, Mathew R, Teo M et al. (2018) Bystander CD8(+) T cells are abundant and phenotypically distinct in human tumour infiltrates. *Nature* 557: 575-579

Steinert EM, Schenkel JM, Fraser KA, Beura LK, Manlove LS, Igyarto BZ, Southern PJ, Masopust D (2015) Quantifying Memory CD8 T Cells Reveals Regionalization of Immunosurveillance. *Cell* 161: 737-49

Stewart EL, Counoupas C, Johansen MD, Nguyen DH, Miemczyk S, Hansbro NG, Ferrell KC, Ashhurst A, Alca S, Ashley C, Steain M, Britton WJ, Hansbro PM, Petrovsky N, Triccas JA (2022) Mucosal immunization with a delta-inulin adjuvanted recombinant spike vaccine elicits lung-resident immune memory and protects mice against SARS-CoV-2. *Mucosal Immunol* 15: 1405-1415

Sun YY, Peng S, Han L, Qiu J, Song L, Tsai Y, Yang B, Roden RB, Trimble CL, Hung CF, Wu TC (2016) Local HPV Recombinant Vaccinia Boost Following Priming with an HPV DNA Vaccine Enhances Local HPV-Specific CD8+ T-cell-Mediated Tumor Control in the Genital Tract. *Clin Cancer Res* 22: 657-69

Thommen DS, Koelzer VH, Herzig P, Roller A, Trefny M, Dimeloe S, Kiialainen A, Hanhart J, Schill C, Hess C, Savic Prince S, Wiese M, Lardinois D, Ho PC, Klein C, Karanikas V, Mertz KD, Schumacher TN, Zippelius A (2018) A transcriptionally and functionally distinct PD-1(+) CD8(+) T cell pool with predictive potential in non-small-cell lung cancer treated with PD-1 blockade. *Nat Med* 24: 994-1004

Valkiers S, de Vrij N, Gielis S, Verbandt S, Ogunjimi B, Laukens K, Meysman P (2022) Recent advances in T-cell receptor repertoire analysis: Bridging the gap with multimodal single-cell RNA sequencing. *ImmunoInformatics* 5: 100009

Virassamy B, Caramia F, Savas P, Sant S, Wang J, Christo SN, Byrne A, Clarke K, Brown E, Teo ZL, von Scheidt B, Freestone D, Gandolfo LC, Weber K, Teply-Szymanski J, Li R, Luen SJ, Denkert C, Loibl S, Lucas O et al. (2023) Intratumoral CD8(+) T cells with a tissue-resident memory phenotype mediate local immunity and immune checkpoint responses in breast cancer. *Cancer Cell* 41: 585-601 e8

Wang B, Wu S, Zeng H, Liu Z, Dong W, He W, Chen X, Dong X, Zheng L, Lin T, Huang J (2015) CD103+ Tumor Infiltrating Lymphocytes Predict a Favorable Prognosis in Urothelial Cell Carcinoma of the Bladder. *J Urol* 194: 556-62

Wang ZQ, Milne K, Derocher H, Webb JR, Nelson BH, Watson PH (2016) CD103 and Intratumoral Immune Response in Breast Cancer. *Clin Cancer Res* 22: 6290-6297

Watanabe R, Gehad A, Yang C, Scott LL, Teague JE, Schlapbach C, Elco CP, Huang V, Matos TR, Kupper TS, Clark RA (2015) Human skin is protected by four functionally and phenotypically discrete populations of resident and recirculating memory T cells. *Sci Transl Med* 7: 279ra39

Workel HH, Komdeur FL, Wouters MC, Plat A, Klip HG, Eggink FA, Wisman GB, Arts HJ, Oonk MH, Mourits MJ, Yigit R, Versluis M, Duiker EW, Hollema H, de Bruyn M, Nijman HW (2016) CD103 defines intraepithelial CD8+ PD1+ tumour-infiltrating lymphocytes of prognostic significance in endometrial adenocarcinoma. *Eur J Cancer* 60: 1-11

Wu J, Madi A, Mieg A, Hotz-Wagenblatt A, Weisshaar N, Ma S, Mohr K, Schlimbach T, Hering M, Borgers H, Cui G (2020) T Cell Factor 1 Suppresses CD103+ Lung Tissue-Resident Memory T Cell Development. *Cell Rep* 31: 107484

Yost KE, Satpathy AT, Wells DK, Qi Y, Wang C, Kageyama R, McNamara KL, Granja JM, Sarin KY, Brown RA, Gupta RK, Curtis C, Bucktrout SL, Davis MM, Chang ALS, Chang HY (2019) Clonal replacement of tumor-specific T cells following PD-1 blockade. *Nat Med* 25: 1251-1259

Zitti B, Hoffer E, Zheng W, Pandey RV, Schlums H, Perinetti Casoni G, Fusi I, Nguyen L, Karner J, Kokkinou E, Carrasco A, Gahm J, Ehrstrom M, Happaniemi S, Keita AV, Hedin CRH, Mjosberg J, Eidsmo L, Bryceson YT (2023) Human skin-resident CD8(+) T cells require RUNX2 and RUNX3 for induction of cytotoxicity and expression of the integrin CD49a. *Immunity* 56: 1285-1302 e7

Figures Legends

Fig 1 : Different immunization routes give rise to distinct subpopulations of resident memory CD8$^+$T lymphocytes with different phenotype and functionality

C57BL/6J mice were immunized with STxB-E7 and aGalcer intranasally (i.n.) or intramuscularly (i.m.) on days 0 and 14, and were sacrificed on day 21. CD8a APCefluo780 (5 µg) was injected (i.v.) 5 min before sacrifice to discriminate between circulating CD8 cells and resident CD8 cells.

(A) Representative flow cytometry plots in BAL (bronchoalveolar lavage fluid) of E7 tetramer-specific CD103$^+$CD49a$^+$ T_{RM}, CD103$^-$CD49a$^+$ T_{RM}, and CD103$^-$CD49a$^-$ Teff, and the frequency of CD69 expression among these populations.

(B) Absolute numbers of (left) E7-tetramer-specific CD8$^+$ and (right) CD103$^+$CD49a$^+$ T_{RM}, CD103$^-$CD49a$^+$ T_{RM}, and Teff CD103$^-$CD49a$^-$ in the BAL. Data are means ± SD. One representative experiment with 3-5 mice from 2 independent experiments is shown. Data were compared between groups via two-sided Mann-Whitney t-tests.

(C) Percentage of PD1 expression among E7-specific CD103$^+$CD49a$^+$ T_{RM}, CD103$^-$CD49a$^+$ T_{RM}, and CD103$^-$CD49a$^-$ Teff in the BAL.

(D) E7-specific CD103$^+$CD49a$^+$ T_{RM}, CD103$^-$CD49a$^+$, and CD103$^-$CD49a$^-$ Teff were sorted from the BAL on day 21 and stimulated (10,000 cells/well) with $E7_{49-57}$ peptide (10 µg/ml) for 18 h. Then, supernatants were harvested and multiplex cytokine detection was performed. Data are

means ± SD. One representative experiment with 3-5 mice from 2 independent experiments is shown. Data were compared within groups via paired one-way ANOVAs with Tukey's multiple comparisons test.

*P<0.05, **P<0.01, ***P<0.001, ****P<0.0001

Figure 2 : Phenotypic analyses of subpopulations of T_{RM} and effector T cells among TILs derived from lung cancer patients.

Fresh biopsies from lung cancer patients (n = 20) were dissociated and digested, and flow cytometry was used to analyze TILs. The number of TILs tested per marker is shown below each figure.

(A) The percentages of T_{RM} subpopulations ($CD103^+CD49a^+$ and $CD49a^+CD103^+$) among $CD8^+$T cells, as well as non-effectors T_{RM} ($CD49a^-CD103^-$) among $CD8^+$T cells are shown.

(B) The percentages of different markers defining T_{RM} (CD69, CXCR6), exhausted T cells (PD-1, Tim-3, CD39), cytotoxicity (GZMB), and proliferation (Ki67) are shown among the two populations of T_{RM} and non-T_{RM} effectors ($CD103^-CD49a^-$). Significance was determined using paired t-tests. P < 0.05 was regarded as statistically significant. *P < 0.05, **P < 0.01, ***P < 0.001; n = 4-20

Figure 3. TCR sharing among the subpopulations of resident memory $CD8^+$T cells

(A) Tracking of the most predominant clonotypes within the $ITGA1^+$(CD49a)/$ITGAE^+$ (CD103) population. Alluvial plots represent the relationships between the frequencies of the 5 most predominant T cell clonotypes detected within the $ITGA1^+/ITGAE^+$ population (right barplot), in the $ITGA1^{neg}/ITGAE^{neg}$ (left barplot) and $ITGA1^+/ITGAE^{neg}$ (middle barplot) populations for each patient. Each square represents the frequency of a clonotype in the corresponding population.

(B) Fold change of the most predominant clonotypes within the $ITGA1^+/ITGAE^+$ population. Dots represent the 5 most predominant T cell clonotypes detected in the $ITGA1^+/ITGAE^+$ population observed using the log2 fold change in $ITGA1^+/ITGAE^+$ (right) and $ITGA1^+/ITGAE^{neg}$ (middle) compared with the $ITGA1^{neg}/ITGAE^{neg}$ (left) cell populations by patient. Each dot is linked across cell populations by a line colored by patient. Statistical analysis was performed using paired Student's t-tests (****P < 0.0001, **P < 0.01).

(C) Jaccard overlap among repetoires was analyzed by generating a heatmap of the Jaccard dissimilarity index calculated across the 3 cell populations: $ITGA1^{neg}/ITGAE^{neg}$ (white), $ITGA1^+/ITGAE^{neg}$ (gray), and $ITGA1^+/ITGAE^+$ (black). The Euclidean distance was used for hierarchical clustering as a color-coded matrix ranging from 0 (minimum dissimilarity) to 1 (maximum dissimilarity).

(D) Morisita horn overlap among repetoires was analyzed by generating a heatmap of the Morisita horn dissimilarity index calculated across the 3 cell populations:

ITGA1^{neg}/ITGAE^{neg}(white), ITGA1^{+}/ITGAE^{neg} (gray), and ITGA1^{+}/ITGAE^{+} (black). The Euclidean distance was used for hierarchical clustering as a color-coded matrix ranging from 0 (minimum dissimilarity) to 1 (maximum dissimilarity). Patients included in this figure are color-coded as patient 1 (orange), patient 2 (green), patient 3 (blue), and patient 4 (red).

Figure 4: NSCLC tumor infiltration by subpopulations of resident memory CD8^{+} T cells.
(A) Representative image of NSCLC tumor infiltration. Multiplexed immunostaining was performed on paraffin-embedded tissues with antibodies to detect CD8, CD103, TCF1, CD49a, and e-cadherin. The InForm® software enabled cell phenotyping and tissue segmentation that was performed by using e-cadherin staining to discriminate between tumor and stromal areas. Automated counting and mapping enabled the phenotyping of T cell subpopulations of non-T_{RM} TILs (defined as CD8^{+}CD49a^{-}CD103^{-}TCF1$^{+/-}$) and of CD8^{+} T_{RM} lymphocytes (defined as CD8^{+}CD49a^{+}CD103^{+}TCF1^{-}, white arrow), CD8^{+}CD49a^{+}CD103^{-}TCF1^{+}, and CD8^{+}CD49a^{+} CD103^{-} TCF1^{-} cells. Original magnification: ×200. Cell numbers (B) and percentages (C) of non-T_{RM} and CD8^{+} T_{RM} were determined via in situ immunofluorescence. Isotype control antibodies were included in each experiment.

Figure 5: Impact of the infiltration of various subpopulations of CD8^{+}T cells in the NSCLC tumor microenvironment on 2nd line therapeutic outcomes.
(A) Forest plot showing the Hazard Ratios (HRs) and 95% confidence intervals computed using a univariate Cox model. The infiltration of several subsets of CD8^{+}T cells and PD-L1 expression were quantified, using the median as a cut-off for dichotomization. Variables are ordered according to decreasing Wald statistic values. The sublocalization of these subpopulations in the stroma or the tumor or not (total) was taken into account. $P < 0.05$ was considered significant (in red).
(B) Kaplan-Meier curves corresponding to the overall survival of patients with NSCLC grouped according to tumoral or stromal infiltration by subpopulations of resident memory CD8^{+} T cells or total TCF1^{+}CD8^{+}T cells and the expression of PD-L1 on tumor cells. Each variable was dichotomized separately based on the median value in order to define low and high groups. Log-rank test values are first displayed together with HRs, 95% confidence intervals, and P-values from the Wald test computed using a univariate Cox model.
(C) Time-dependent ROC curves were used to analyze the sensitivity and specificity of the two subpopulations of resident memory CD8+ T cells, total CD8^{+}T cells, TCF1^{+}CD8^{+}T cells, and PD-L1 when predicting 2-year overall survival. For each variable, only patients whose variable values were located in the extreme tertiles of the corresponding distribution were included. The resulting area under the curve (AUC) values are shown

Figure 6: The clinical impact of the infiltration of various subpopulations of CD8+ T cells in the NSCLC tumor microenvironment in a validation cohort

(A) Forest plot representing Cox overall survival regression in NSCLC patients (n = 36). The infiltration of several subsets of $CD8^+$ T cells was quantified using the median as a cut-off. The sublocalization of these subpopulations in the stroma or the tumor or not (total) was taken into account. $P < 0.05$ was considered significant

(B) Kaplan-Meier analyses of the overall survival of patients with NSCLC depending on their level of intratumoral $CD49a^+CD103^+CD8^+$ T cells dichotomized with the median. Statistical analyses were performed with the log-rank test.

(C) Forest plot representing Cox progression-free survival regression in NSCLC patients (n = 36). The infiltration of several subsets of $CD8^+$ T cells was quantified using the median as a cut-off. The sublocalization of these subpopulations in the stroma or the tumor or not (total) was taken into account. $P < 0.05$ was considered significant

.

Variable	N	HR	95%CI	P
TCF-1$^+$CD8$^+$ Stroma	52	0.98	(0.96,1.00)	0.12
PD-L1	52	0.99	(0.98,1.00)	0.08
CD49a$^+$CD103$^+$CD8$^+$T cells (Tumor)	52			
Low Tertile	14			
High+Inter Tertile	38	0.39	(0.16,0.92)	0.03

Table 1 : Multivariable model adjusted for PD-L1 level and total stromal TCF-1$^+$CD8$^+$ T cells

Using Cox proportional Hazard Model, the value of intratumoral CD49a$^+$CD103$^+$CD8$^+$T cells (divided in tertile) in predicting overall survival was evaluated in a multivariate analysis adjusted for PD-L1 and total TCF-1$^+$CD8$^+$T cells as continuous variables

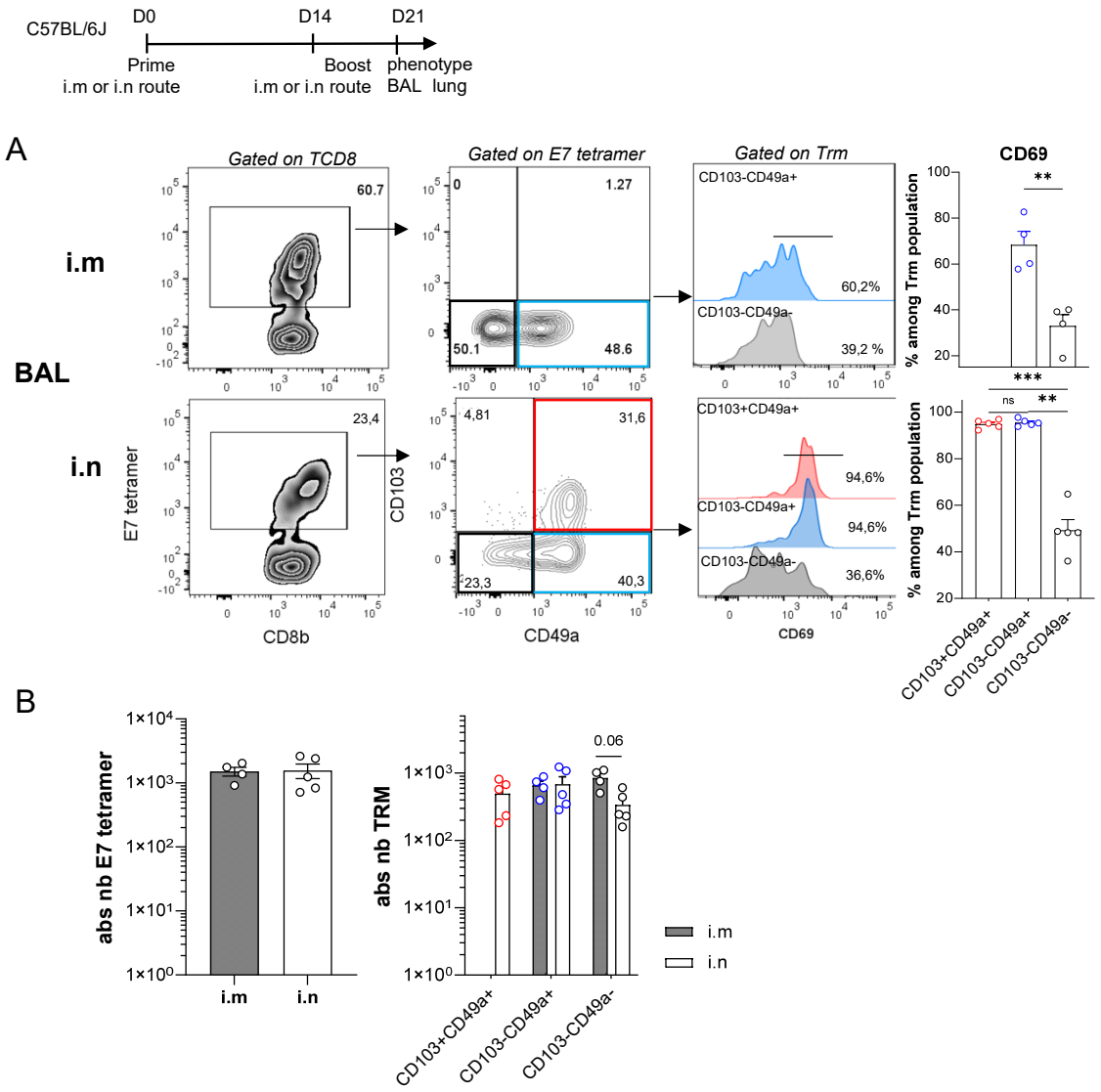

Figure 1

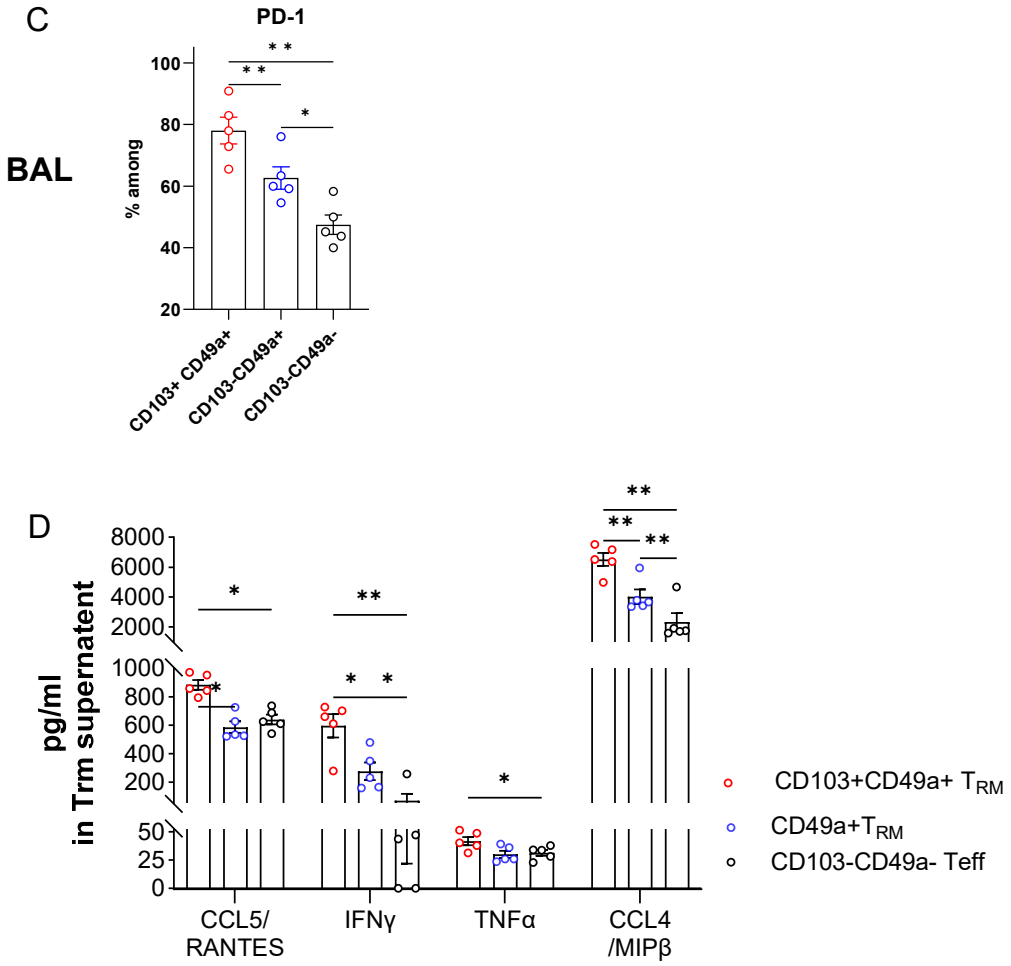

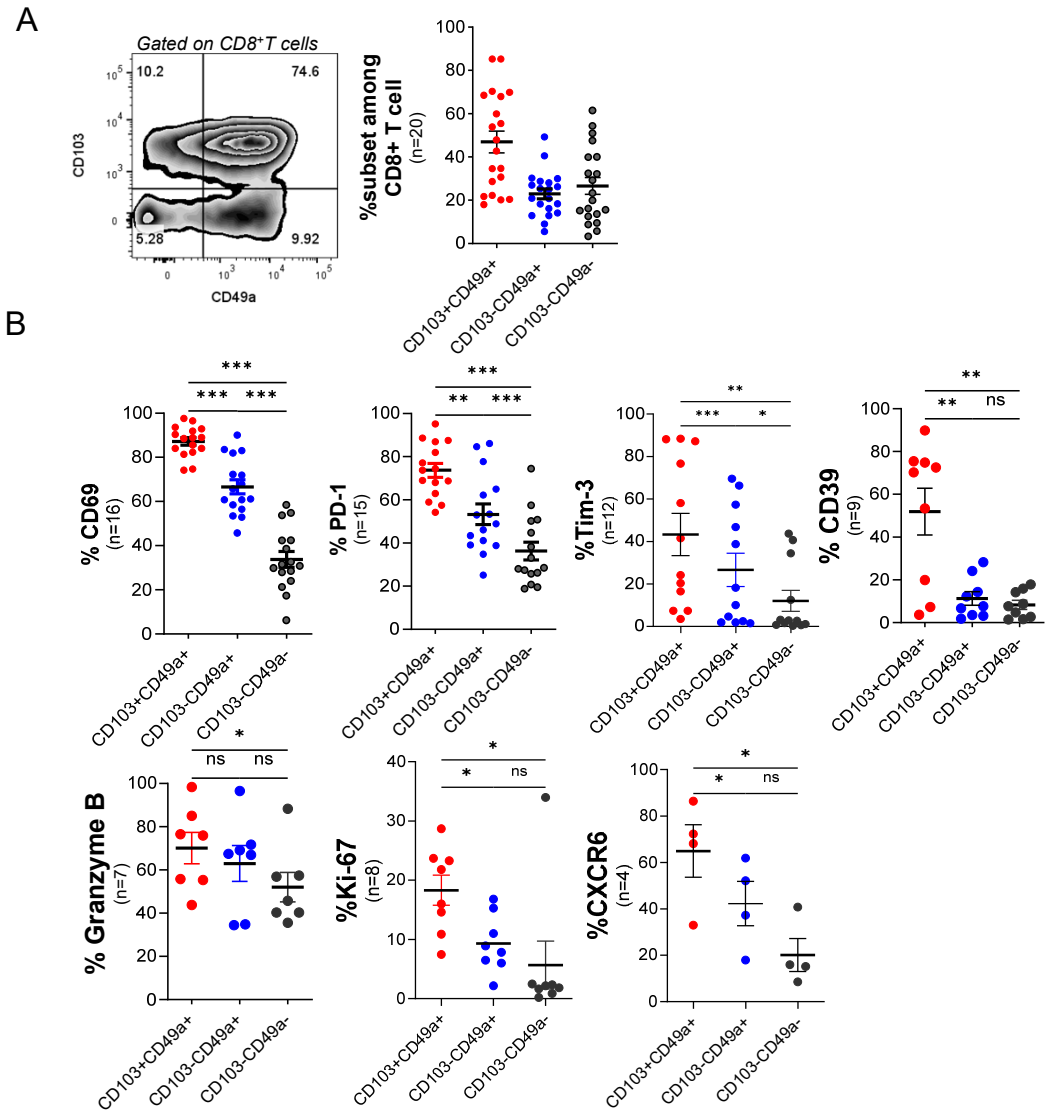

Figure 2

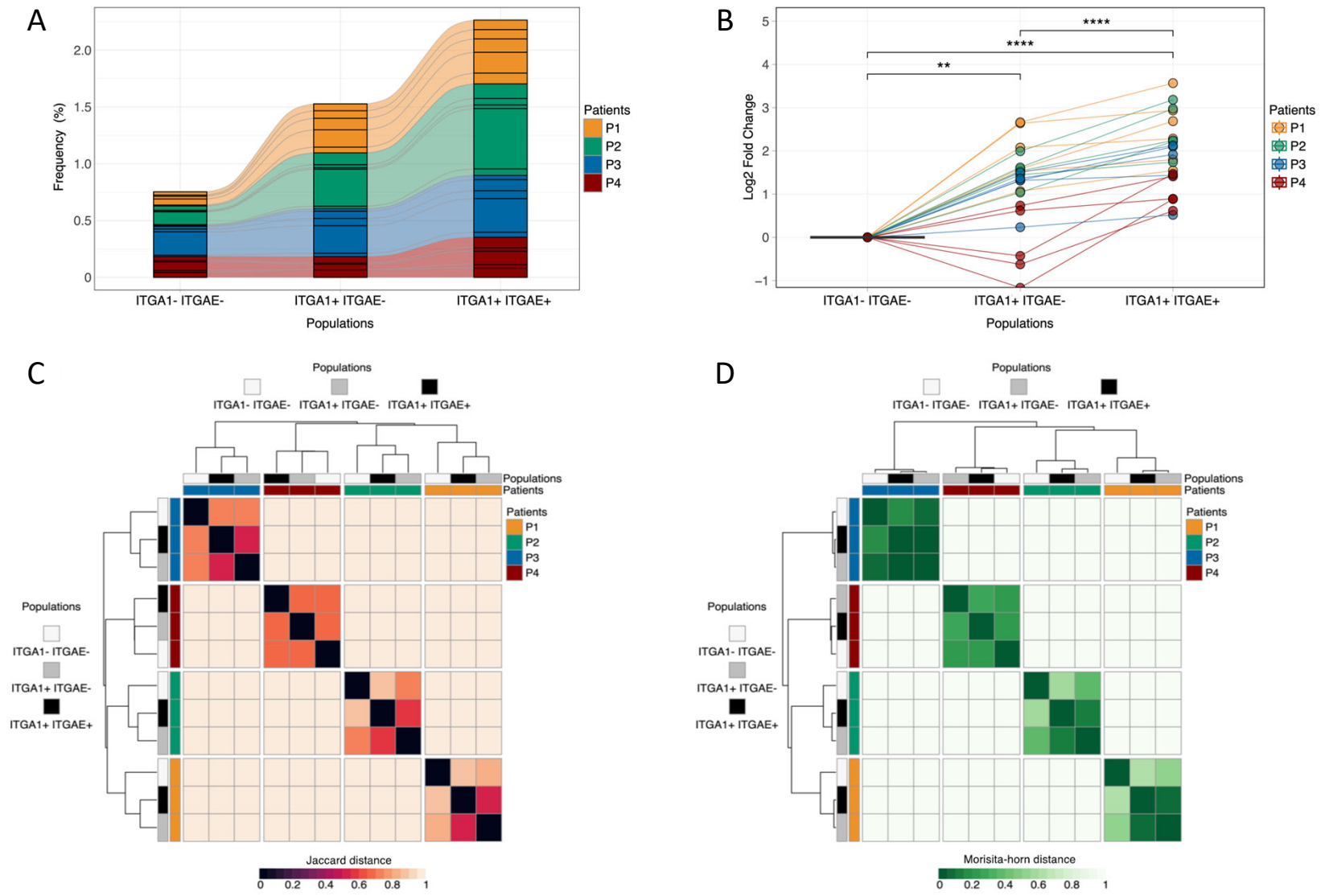

Figure 3

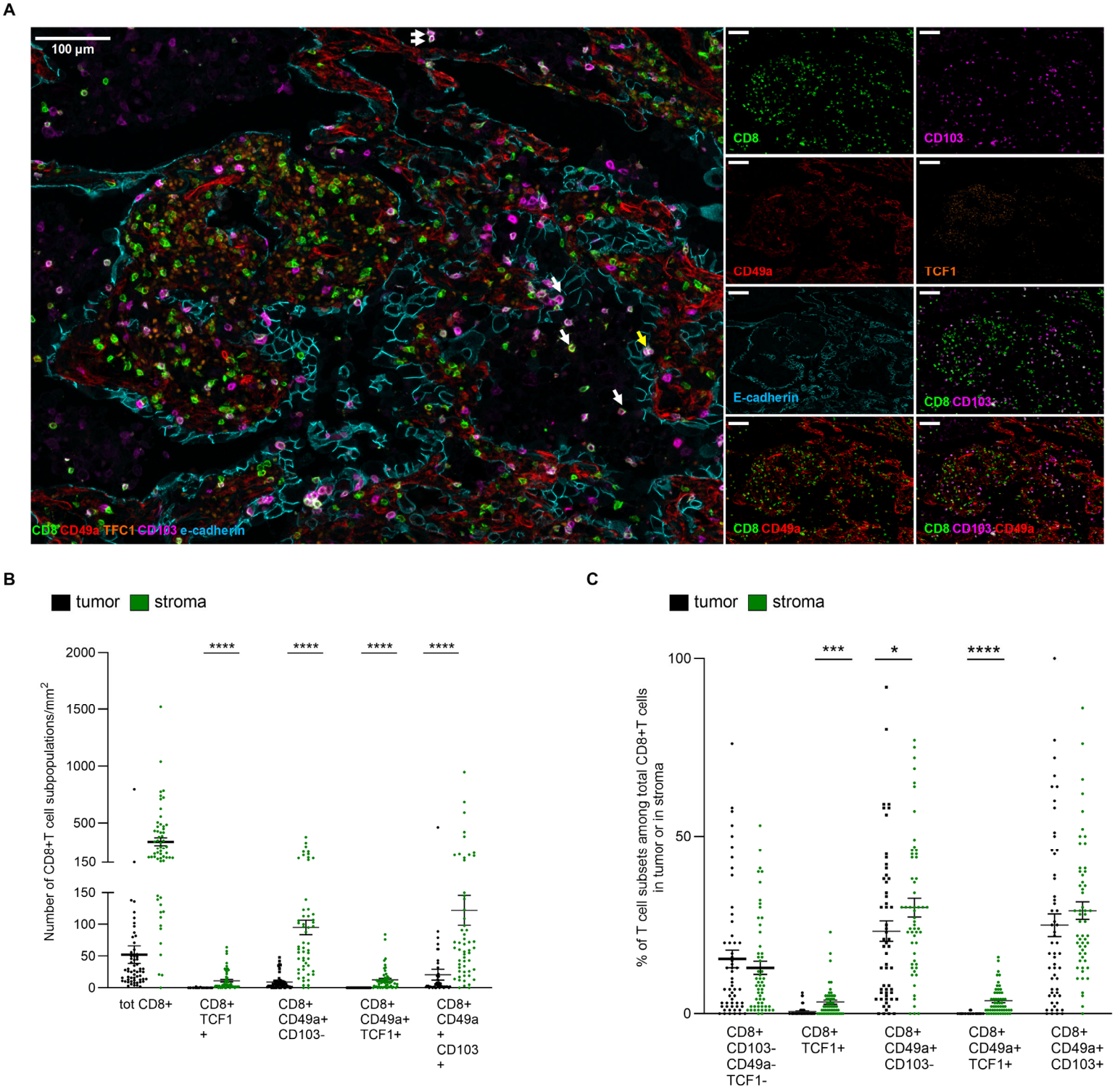

Figure 4

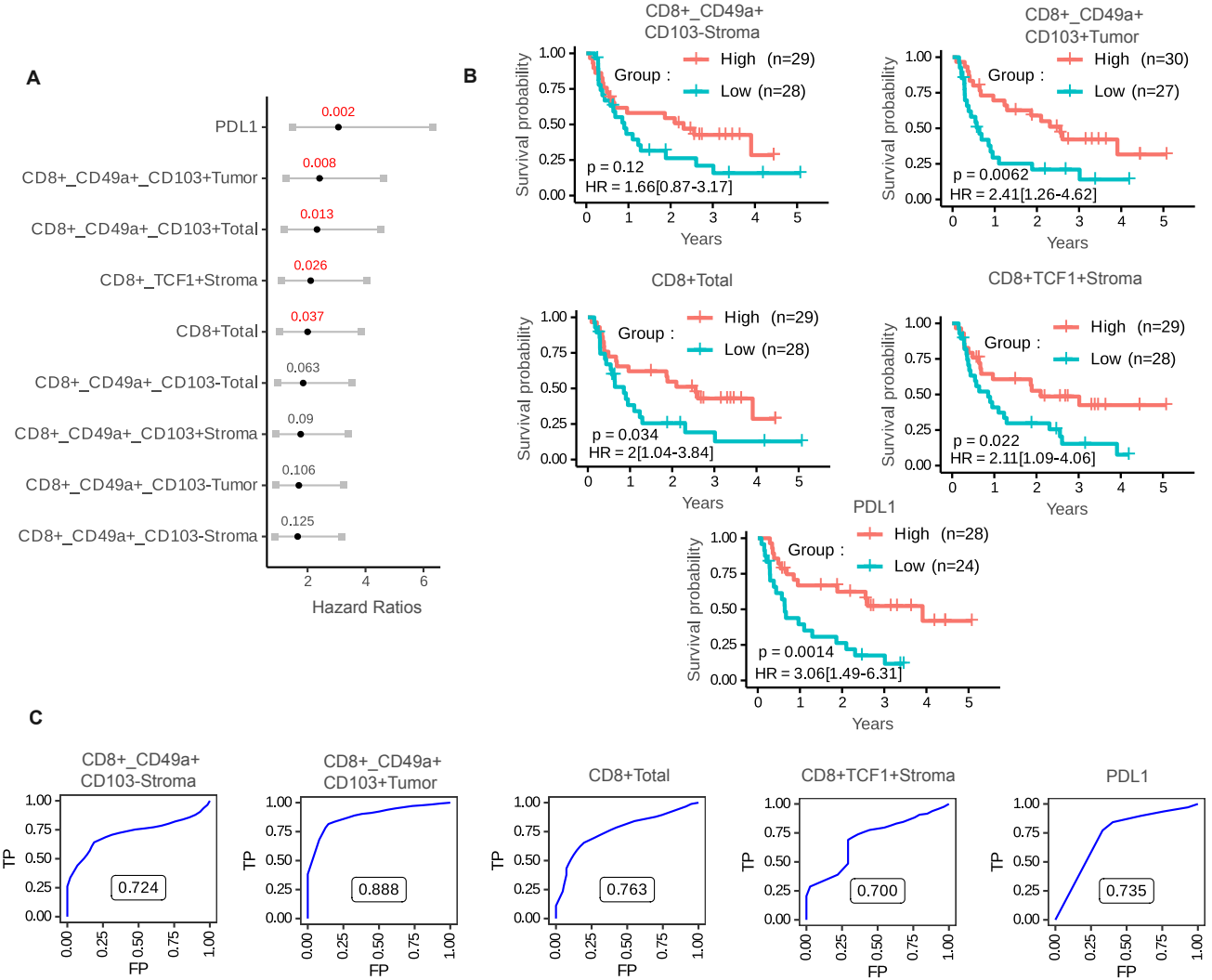
A
PDL1
CD8+_CD49a+_CD103+Tumor
CD8+_CD49a+_CD103+Total
CD8+_TCF1+Stroma
CD8+Total
CD8+_CD49a+_CD103-Total
CD8+_CD49a+_CD103+Stroma
CD8+_CD49a+_CD103-Tumor
CD8+_CD49a+_CD103-Stroma
0.002
0.008
0.013
0.026
0.037
0.063
0.09
0.106
0.125
2
4
6
Hazard Ratios
B
CD8+_CD49a+ CD103-Stroma
Group :
High (n=29)
Low (n=28)
p = 0.12
HR = 1.66[0.87-3.17]
CD8+_CD49a+ CD103+Tumor
High (n=30)
Low (n=27)
p = 0.0062
HR = 2.41[1.26-4.62]
CD8+Total
High (n=29)
Low (n=28)
p = 0.034
HR = 2[1.04-3.84]
CD8+TCF1+Stroma
High (n=29)
Low (n=28)
p = 0.022
HR = 2.11[1.09-4.06]
PDL1
High (n=28)
Low (n=24)
p = 0.0014
HR = 3.06[1.49-6.31]
Survival probability
Years
C
CD8+_CD49a+ CD103-Stroma
0.724
CD8+_CD49a+ CD103+Tumor
0.888
CD8+Total
0.763
CD8+TCF1+Stroma
0.700
PDL1
0.735
TP
FP

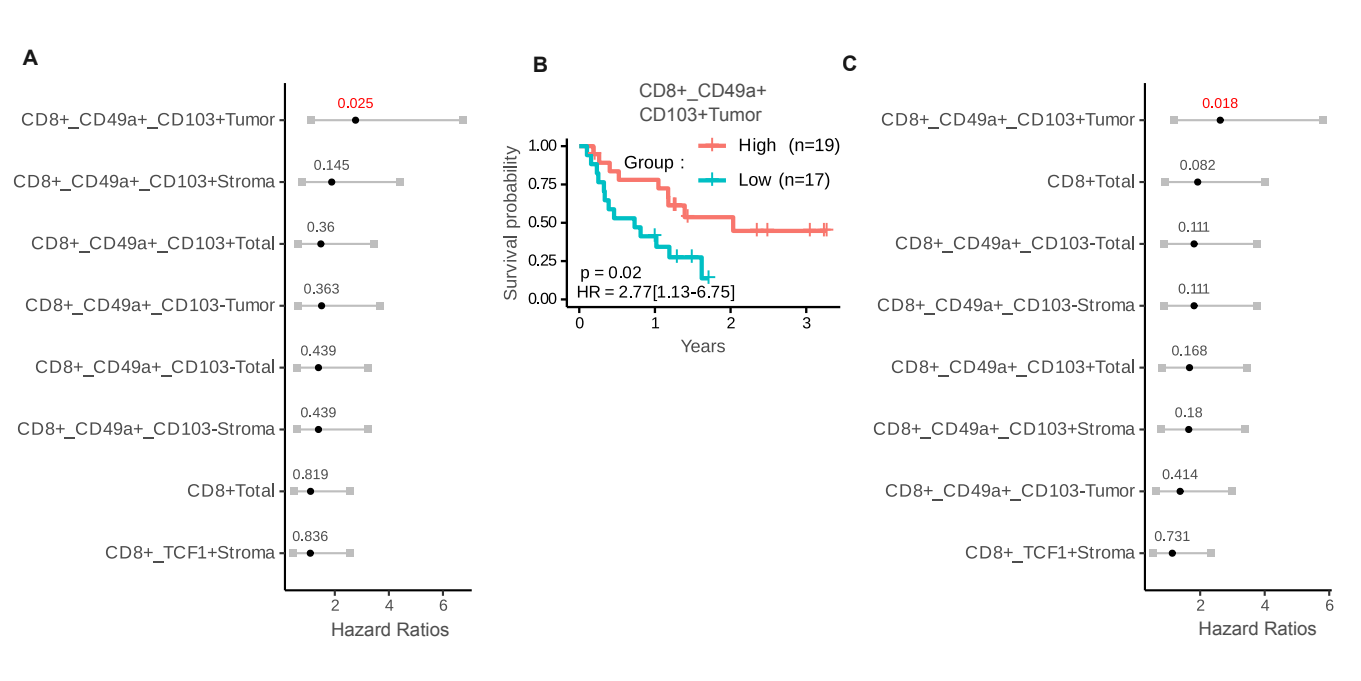
A
CD8+_CD49a+_CD103+Tumor
CD8+_CD49a+_CD103+Stroma
CD8+_CD49a+_CD103+Total
CD8+_CD49a+_CD103-Tumor
CD8+_CD49a+_CD103-Total
CD8+_CD49a+_CD103-Stroma
CD8+Total
CD8+_TCF1+Stroma
0.025
0.145
0.36
0.363
0.439
0.439
0.819
0.836
2
4
6
Hazard Ratios
B
CD8+_CD49a+
CD103+Tumor
Survival probability
1.00
0.75
0.50
0.25
0.00
Group :
High (n=19)
Low (n=17)
p = 0.02
HR = 2.77[1.13-6.75]
0
1
2
3
Years
C
CD8+_CD49a+_CD103+Tumor
CD8+Total
CD8+_CD49a+_CD103-Total
CD8+_CD49a+_CD103-Stroma
CD8+_CD49a+_CD103+Total
CD8+_CD49a+_CD103+Stroma
CD8+_CD49a+_CD103-Tumor
CD8+_TCF1+Stroma
0.018
0.082
0.111
0.111
0.168
0.18
0.414
0.731
2
4
6
Hazard Ratios